Self-consistent calculation and analysis of the optical properties and modulated doping in GaAs/AlGaAs quantum wells

John Alexander Gil Corrales

Submitted to the University of Antioquia in fulfillment of the Physics Master requirements program

Advisor:
PhD Álvaro Morales Aramburo
Co-Advisor:
PhD Carlos Alberto Duque Echeverri

Research group:
Condensed Matter-UdeA

University of Antioquia
Faculty of Exact and Natural Sciences, Institute of Physics
Medellín, Colombia
2023

Publication

[1] Gil-Corrales, J. A.; Morales, A. L.; Duque, C. A. Self-Consistent Study of GaAs/AlGaAs Quantum Wells with Modulated Doping, *Nanomaterials* **2023**, 13, 913.

Abstract

In this work, physics characterization and analysis of a GaAs quantum well with AlGaAs barriers is carried out, considering an interior doped layer. An analysis of the probability density, the energy spectrum, and the electronic density has been carried out, solving in a self-consistent way the Schrödinger, Poisson, and charge neutrality equations. Between the characterization, the system response under geometric changes in the well width and non-geometric changes such as the position and doped layer width and the donor's density were reviewed. All the second-order differential equations have been solved using the finite-difference method. Finally, with the obtained wave functions and energies, the optical absorption coefficient and the electromagnetically induced transparency between the first three confined states have been calculated. The results show the possibility of tuning the optical absorption coefficient and the electromagnetically induced transparency via changes in the system geometry and doped layer characteristics.

Contents

List of symbols

Abbreviations

Abbreviation	**Name**
QD	Quantum dot
QW	Quantum well
OAC	Optical absorption coefficient
FDM	Finite difference method
EIT	Electromagnetic induced transparency

1. Introduction

Quantum wells (QWs) are semiconductor heterostructures that confine electrons (or holes) in one spatial dimension, being free in the other two dimensions. The study of these systems was promoted mainly from the second half of the last century due to the invention of experimental techniques such as molecular beam epitaxy (MBE) in 1968 at Bell Labs by Alfred Cho and John Artur [1, 2] that allowed the possibility of growing very thin and high-quality layers. Even today, QWs are widely studied both theoretically and experimentally due to their multiple applications. In the case of $Al_{0.3}Ga_{0.7}As/GaAs/Al_{0.3}Ga_{0.7}As$ heteroestructure, a quantum well is formed in the conduction band since the gap of $Al_{0.3}Ga_{0.7}As$ is greater than the GaAs gap. An immediate consequence of this type of confinement is that the energy levels in the confinement direction become discrete and have a direct dependence on well width, and donor density, among other parameters.

It is important to mention some of the multiple applications of QWs, among which stand-out works in the optoelectronics field, such as the theoretical work developed in 2022 by Aissat *et al.* [3] in which multiple quantum wells (MQWs) were implanted inside the intrinsic region in a solar cell type device based on InGaAsN/GaAs to improve efficiency by taking advantage of the low energy photon absorption. In this work, Aissat *et al.* obtained a theoretical external quantum efficiency (EQE) greater than 80 %. It should be clarified that some of the first works in which the use of structures such as multiple QWs is proposed for applications in devices such as solar cells were developed in the 80s, in pioneering works such as that of C. J. Summers and K. F. Brennan [4]. In this same optoelectronics field, Roy *et al.* [5] analyzed the effect of dark current from the theoretical point of view for the development of a CdS/ZnSe photodetector for mid-infrared based on an array of MQWs; their results showed a high

detectivity of this system compared to other materials and different composition. In the experimental field, in 2021, Yu and Dang [6] synthesized colloidal metal chalcogenide quantum wells (CQWs) for laser applications ten years after the successful synthesis of two-dimensional colloidal systems; in this work, the authors categorized different systems according to the confinement of photons and laser mechanisms, such as amplification of spontaneous emission, a laser with a cavity, and a multiphoton-pumped laser.

It is worth mentioning some applications in more diverse fields, such as the work of Hu and Zhang [7], who in 2020 proposed a ZnO QWs topological insulator piezoelectric device. They found that through stress, the induced piezoelectric field can cause the QWs to behave as topological insulators; this behavior depends to a large extent on the QWs width. Regarding the QWs application in electronics, considering some more recent works, in 2022, Zhou *et al.* [8] used machine learning methods to demonstrate that through the application of neural networks, it is possible to solve the wavelength of intersubband transitions in piezo-phototronic GaN/AlN transistors since their hidden layers can be accurately approximated by any continuous function. In 2022, in an interesting experimental work by Park *et al.* [9] studied the effective mobility of InGaAs/InAlAs QW for direct application in high electron mobility transistors (HEMTs) on an InP substrate. They achieved a significant reduction in the gate leakage current, which allows for obtaining more precise measures of effective mobility.

In the applications mentioned above, QWs or MQWs systems based on various materials are reported. Systems based on GaAs/AlGaAs are particularly interesting since they are widely studied materials. Due to their particular characteristics of tuning electronic properties with external parameters, they are of great use for multiple applications in various fields. In 2023, Türkoglu *et al.* [10] investigated the photoluminescence of GaAs/AlGaAs MQWs grown by metal-organic vapor phase epitaxy (MOVPE); they analyzed the transition between bands in the structure and their changes under different temperatures and external electric fields. In 2022 Makhov *et al.* [11] experimentally investigated the effect of the photon current drag in the mid-infrared range corresponding to the intersubband optical electron transitions in GaAs/AlGaAs QWs at room

temperature; they studied the dependence of the change in refractive index in the lateral current for different polarizations.

Currently, this type of material is of great interest since it allows optoelectronic applications at terahertz frequencies. AL-Naghmaish *et al.* [12] studied the optical response of a system of QWs as photodetectors under the effect of magnetic and electric fields and intense laser fields. Their work demonstrated the possibility of adjusting and tuning the absorption coefficient and the refractive index for terahertz applications. The recent advances in these materials have not been given exclusively from the theoretical point of view. It is necessary to highlight the advances in experimental techniques that have allowed a better characterization of these heterostructures [13, 14]. Just to reference one of these works, in 2021, Zhang *et al.* [15] performed the insertion of GaAs layers to improve the properties of InGaAs/AlGaAs MQWs grown by metal-organic chemical vapor deposition. The study showed that when the GaAs layer was approximately 6 nm, the maximum properties of the system were found.

When characterizing a QWs system, either for a possible application in an optoelectronic device or as an active element in an electrical circuit, it is necessary to consider materials that include doping since, when doping the material, the electronic transport properties are amplified as are experimentally measurable characteristics such as electric current, conductance, etc. Thus, to obtain a better fit between the theoretical and experimental results, it is necessary to consider QWs models that consider the electrostatic potential generated by a donor density. In 2023, Dakhlaoui *et al.* [16] numerically studied the optical response in Manning-like GaAs/AlGaAs double QWs, including the effects of doped impurities. They added an n-doped layer in two different positions of the potential. Among the reported results, there is evidence of a loss of degeneracy of the energy levels depending on the position of the doped layer and the density of donors; this feature significantly modifies the optical properties of the system. In 2021 Sadonov *et al.* [17] investigated both theoretically and experimentally the dependence of the electron transport properties of a two-dimensional electron gas on sheet doping concentration in one-sided δ-doped pseudomorphic AlGaAs/InGaAs/GaAs QWs. Among the results of their re-

port, the dependence of the transport relaxation times with n_H (ionized donors concentration) exhibit a non-monotonic behavior due to the competition of the Fermi momentum increase and the scattering angle due to the n_H variation.

These heterostructures are widely characterized by their optical properties, such as linear and nonlinear optical absorption coefficient, electromagnetically induced transparency (EIT), and change in refractive index, among others. This is evidenced by recent works such as that of Rodríguez-Magdaleno *et al.* [18] in which a theoretical study of the electronic structure and the inter-subbands related optical absorption coefficient for symmetrical double delta-doped GaAs QW was carried out. Among the reported results, the modification of the absorption peak position due to the presence of donor impurity atom stands out. In another interesting theoretical work, Jayarubi *et al.* [19] calculated the nonlinear optical absorption coefficient and the EIT in GaAs/InAs/GaAs QWs. The optical susceptibilities, the detuning parameters, and the Rabi frequency were also analyzed. In general, it is a complete work from the theory point of view to understand the effect of EIT on low-dimensional heterostructures.

Being clear that the system of GaAs/AlGaAs QWs with internal doping is a problem of wide current development, this work characterizes a GaAs QW with AlGaAs barriers, considering the modification in the bottom of the conduction band due to the electrostatic potential generated by a δ-doped layer. The study considers variations in the energy spectrum, probability density, electron density, and Fermi level. In this work, geometric modifications such as the QW width and non-geometric modifications such as the doped region width and the doped layer position are made.

Due to the significant growth of experimental techniques in recent years, it is currently possible to grow very thin doped regions (delta type) of very precise widths and of high quality inside heterostructures such as QWs of various materials, as evidenced by works such as that of F. Ishikawa *et al.* [20] who studied the energy-band engineering with nitrogen delta δ-doping in GaAs-related quantum structures. In the same way, by means of techniques such as molecular beam epitaxy, it is possible to control the position of doped layers, a reference

to the application of the said method is presented in the report by H. Khmissi *et al.* [21]. In 2018 S. Kang *et al.* [22] used the Si δ-doping technique to fabricate high-performance GaAs tunnel diodes (TDs).

By including a doped region inside a heterostructure, some of its properties can be improved, for example, the cathodoluminescence (CL) in InP quantum dots grown on an InAlP matrix was improved about 16 times by mean of modulation of the position of a silicon-doped delta layer, this was an experimental work by X. B. Zhang *et al.* [23]. In another interesting report, X. Chen *et al.* [24] performed a characterization of a GaAs-based high-speed and high-sensitivity delta-doped resonant cavity-enhanced heterostructure metal-semiconductor-metal (HMSM) photodetector, finding that the growth of a doped delta layer inside the heterostructure improves the photocurrent spectral response, dark current, time response, and capacitance–voltage measurements compared to undoped systems. To mention one last report, V. V. Vainberg *et al.* [25] experimentally modulated the position of the delta layer, inside and outside a GaAs/InGaAs/GaAs quantum well, finding a significant increase in electron mobility when the delta layer is located in barrier regions compared to measurements of the delta layer inside the quantum well.

As an application of the findings (eigenvalues and eigenfunctions), the linear absorption coefficient and the EIT have been calculated. A self-consistent method combined with the finite difference method (FDM) is used to solve the coupled Schrödinger, Poisson, and charge neutrality equations. The work is organized as follows: In Chapter 2: the theoretical model is presented, including the Optical absorption theory, the self-consistent method, EIT theory, and the finite difference method. In Chapter 3: the results an discussion is presented as follow: energies and probability density, Hartree potential, linear optical absorption coefficient and EIT results. Finally, in Chapter 4 the conclusions are given, and in the annexes section, the self-consistent code used for the calculations has been included. The objectives of this research work are explicitly mentioned below:

General Objective

To study the optical properties of GaAs/AlGaAs quantum wells with modulated doping by implementing a self-consistent procedure.

Specific objectives

(1) Implement a self-consistent code to numerically solve the Schrödinger and Poisson equations in a GaAs/AlGaAs quantum well with modulated doping.

(2) Calculate the eigenvalues, wave functions and probability densities in the studied system.

(3) Calculate the Fermi level, potential, Hartree potential, and electron density after reaching the self-consistency of the system.

(4) Study the system response under changes in geometric parameters such as the well width.

(5) Study the system response under changes in non-geometric parameters such as the width and position of the doped delta layer, and the donor density.

(6) Discuss the changes in Hartree potential and electron density with the previously mentioned changes in parameters.

(7) Calculate the linear optical absorption and the electromagnetic induced transparency taking the three lowest levels.

References

[1] Arthur, J. R. Interaction of Ga and As2 Molecular Beams with GaAs Surfaces, *J. Appl. Phys.* **1968**, *39*, 4032.

[2] Cho, A. Y.; Arthur, J. R. Molecular Beam Epitaxy, *Prog. Solid. State Ch.* **1975**, *10*, 157-191.

[3] Aissat, A.; Bestam, R.; Boubakeur, M.; Vilcot, J. P. Development of the multi-quantum wells structures based on In_xGa_{1-x} $As_{1-y}N_y$/GaAs for solar cells applications, *Micro and Nanostruct.* **2022**, *170*, 207369.

[4] Summers, C. J.; Brennan, K. F. Variably spaced superlattice energy filter, a new device design concept for highenergy electron injection, *Appl. Phys. Lett.* **1986**, *48*, 806.

[5] Roy, B.; Billaha, M. A.; Dutta, R.; Mukherjee, D. Analysis of dark current and detectivity of CdS/ZnSe Based multiple quantum well photodetector for mid-infrared applications, *Physica E Low Dimens. Syst. Nanostruct.* **2023**, *147*, 115614.

[6] Yu, J.; Dang, C. Colloidal Metal Chalcogenide Quantum Wells for Laser Applications, *Cell Rep. Phys. Sci.* **2021**, *2*, 100308.

[7] Hu, G.; Zhang, Y. Quantum piezotronic devices based on ZnO/CdO quantum well topological insulator, *Nano Energy* **2020**, *77*, 105154.

[8] Zhou, Y.; Dan, M.; Shao, Y.; Zhang, Y. Deep-neural-network solution of piezo-phototronic transistor based on GaN/AlN quantum wells, *Nano Energy* **2022**, *101*, 107586.

[9] Park, W.-S.; Kim, J.-G.; Yun, S.-W.; Jeong, H.-S.; Jo, H.-B.; Kim, T.-W.; Tsutsumi, T.; Sugiyama, H.; Matsuzaki, H.; Kim, D.-H. Extraction of effective mobility of $In_{0.8}Ga_{0.2}As/In_{0.52}Al_{0.48}As$ quantum well high-electron-mobility transistors on InP substrate, *Solid State Electron.* **2022**, *197*, 108446.

[10] Türkoglu, A.; Ergün, Y.; Ungan, F. Investigation of the electro-optical characteristics of GaAs/AlGaAs multiple quantum well grown by metal-organic vapor phase epitaxy, *J. Mol. Struct.* **2023**, *1272*, 134202.

[11] Makhov, I. S.; Budkin, G. V.; Graf, S. V.; Firsov, D. A. Current induced drag of photons in GaAs/AlGaAs quantum wells, *Micro and Nanostruct.* **2022**, *167*, 207288.

[12] AL-Naghmaish, A.; Dakhlaoui, H.; Ghrib, T.; Wong, B. M. Effects of magnetic, electric, and intense laser fields on the optical properties of AlGaAs/GaAs quantum wells for terahertz photodetectors, *Phys. B: Condens. Matter* **2022**, *635*, 413838.

[13] Touraton, M.-L.; Martin, M.; David, S.; Bernier, N.; Rochat, N.; Moeyaert, J.; Loup, V.; Boeuf, F.; Jany, C.; Dutartre, D.; Baron, T. Selective epitaxial growth of AlGaAs/GaAs heterostructures on 300 mm Si (001) for red optical emission, *Thin Solid Films* **2021**, *721*, 138541.

[14] Bietti, S.; Cavigli, L.; Minari, S.; Adorno, S.; Isella, G.; Vinattieri, A.; Gurioli, M.; Sanguinetti, S. Effects of As pressure on the quality of GaAs/AlGaAs quantum dots grown on silicon by droplet epitaxy, *J. Cryst. Growth* **2013**, *378*, 497–500.

[15] Zhang, B.; Wang, H.; Wang, X.; Wang, Q.; Fan, J.; Zou, Y.; Ma, X. Effect of GaAs insertion layer on the properties improvement of InGaAs/AlGaAs multiple quantum wells grown by metal-organic chemical vapor deposition, *J. Alloys Compd.* **2021**, *872*, 159470.

[16] Dakhlaoui, H.; Belhadj, W.; Durmuslar, A. S.; Ungan, F.; Abdelkader, A. Numerical study of optical absorption coefficients in Manning-like Al-

GaAs/GaAs double quantum wells: Effects of doped impurities, *Physica E Low Dimens. Syst. Nanostruct.* **2023**, *147*, 115623.

[17] Safonov, D. A.; Klochkov, A. N.; Vinichenko, A. N.; Sibirmovsky, Y. D.; Kargin, N. I.; Vasil'evskii, I. S. Electron effective masses, nonparabolicity and scattering times in one side delta-doped PHEMT AlGaAs/InGaAs/GaAs quantum wells at high electron density limit, *Physica E Low Dimens. Syst. Nanostruct.* **2021**, *133*, 114787.

[18] Rodríguez-Magdaleno, K. A.; Turkoglu, A.; Ungan, F.; Mora-Ramos, M. E.; Martínez-Orozco, J. C. Donor impurity atom effect on the inter-subband absorption coefficient for symmetric double n-type δ-doped GaAs quantum well, *Superlattices Microstruct.* **2021**, *156*, 106988.

[19] Jayarubia, J.; Petera, A. J.; Lee, C. W. Electromagnetically induced transparency in a GaAs/InAs/GaAs quantum well, *Physica B Condens* **2018**, *550*, 184–188.

[20] Ishikawa, F.; Furuse, S.; Sumiya, K.; Kinoshita, A.; Morifuji, M. Nitrogen δ-doping for band engineering of GaAs-related quantum structures, *Appl. Phys.* **2012**, *111*, 053512.

[21] Khmissi, H.; Baira, M.; Sfaxi, L.; Bouzaïene, L.; Saidi, F.; Bru-Chevallier, C.; Maaref, H. Optical investigation of InAs quantum dots inserted in AlGaAs/GaAs modulation doped heterostructure, *Appl. Phys.* **2011**, *109*, 054316.

[22] Kang, S.; Ju, G. W.; Min, J.-W.; Lee, D.-S.; Lee, Y. T.; Kim, H. J.; Park, K. Detailed analysis and performance limiting mechanism of Si delta-doped GaAs tunnel diode grown by MBE, *Jpn J Appl Phys.* **2018**, *57*, 120306.

[23] Zhang, X. B.; Heller, R. D.; Noh, M. S.; Dupuis, R. D. Effect of Si delta doping on the luminescence properties of InP/InAlP quantum dots, *Appl. Phys. Lett.* **2003**, *82*, 4343.

[24] Chen, X.; Nabet, B.; Zhao, X.; Huang, H.-J.; Cola, A.; Quaranta, F.; Taurino, A.; Currie, M. Optical and Electrical Characterization of GaAs-Based

High-Speed and High-Sensitivity Delta-Doped Resonant Cavity-Enhanced HMSM Photodetector, *T-ED* **2005**, *52*, 454-464.

[25] Vainberg, V. V.; Pylypchuk, A. S.; Baidus, N. V.; Zvonkov. B. N. Electron mobility in the GaAs/InGaAs/GaAs quantum wells, *Semicond. Phys. Quantum Electron. Optoelectron.* **2013**, *16*, 152-161.

2. General theoretical framework

The system to be studied corresponds to a GaAs quantum well with $Al_{0.3}Ga_{0.7}As$ barriers, as shown in Figure **2-1**, this is characterized by a height V_0 and width L centered at the x-axis origin. The L-parameter is the well-width centered at the x-axis origin. The system presents an n-type doped layer located at a distance ξ from the origin and of width δ, represented by the green rectangle.

The calculation presented will be considered at room temperature since one of the main objectives of the work is to understand the physics of this type of heterostructures and in this way, these could be implemented more directly in electronic devices or in applications of more common use (it is more difficult to find an application from a device that only works at low temperatures). The effect of working at lower temperatures in this type of system has not been explored by means of this model, however, a decrease in the occupancy of the confined states could be expected as a direct effect of the decrease in temperature, because the self-consistent Fermi level is proportional to this. As a consequence of the above, the density of electrons occupying discrete states would decrease, which could impair the characterization of the system by means of optics, since the number of charge carriers available to perform transitions would decrease.

For room temperature, it is reasonable to consider a total ionization of the donor atoms, the above because for the implementation of this type of heterostructure in practical applications or in devices, it is necessary to have a set of half-occupied states that increase electronic mobility through the system, that is, to have a certain electronic occupancy in the conduction band. Although

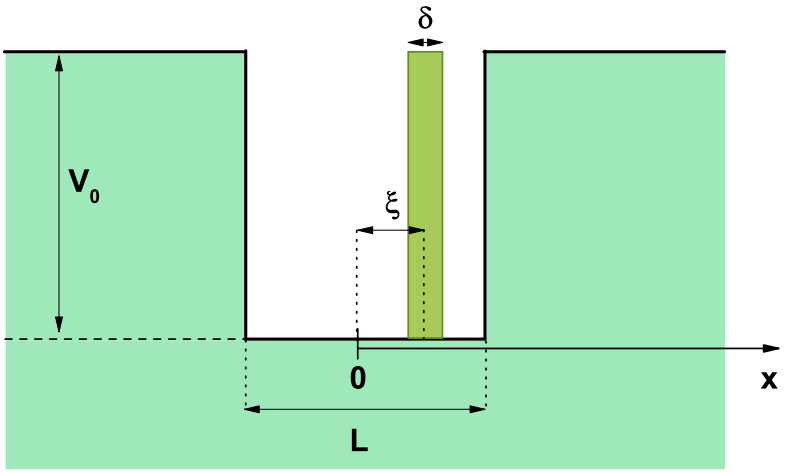

Figure 2-1.: Schematic view corresponding to a quantum well of height V_0 and width L centered at the x-axis origin. The doped delta layer of δ-width located at a ξ-distance from the origin of the coordinates is shown in dark-green.

complete ionization has been assumed in this work, it is clear that the percentage of ionized atoms is dependent on the system temperature and the donor density [1]. In order for theoretical calculations to be useful for potential applications, we have worked at room temperature, at this temperature, for GaAs it is possible to consider a "relatively high ionization" even taking into account the increase in impurity ionization energy for the case of one-dimensional confinement. References [3, 6, 7] present various quantum wells of different materials in which total ionization with different densities at room temperature has been considered, reporting very interesting results.
It is possible to determine a relationship to find the relative number of electrons in the donor state, starting from the relationship for the probability function of electrons occupying the donor state:

$$n_d = \frac{N_d}{1 + (1/2)\exp\left(\frac{E_d - E_f}{k_B T}\right)}, \tag{2-1}$$

where $n_d = N_d - N_d^+$ is the electron density occupying the donor level and E_d

is the donor energy level, N_d is the donor density atoms, and N_d^+ is the density of ionized donors in the case in which $(E_d - E_f) \gg k_B\,T$ is fulfilled, the last expression is reduced to:

$$n_d = 2N_d \exp\left(-\frac{(E_d - E_f)}{k_B\,T}\right), \tag{2-2}$$

this approximation (Boltzmann approximation) is also valid for electrons in the conduction band:

$$n_0 = 2N_C \exp\left(-\frac{(E_C - E_f)}{k_B\,T}\right), \tag{2-3}$$

where N_C is the effective density of states in the conduction band and E_C is the conduction level. Now we can determine the relative number of electrons in the donor state compared to the total number of electrons,

$$\frac{n_d}{n_d + n_0} = \frac{1}{1 + \frac{N_C}{2N_d}\exp\left(-\frac{(E_C - E_d)}{k_B\,T}\right)}, \tag{2-4}$$

As an example, for Si at room temperature, $N_C = 3.2 \times 10^{19}\,\mathrm{cm}^{-3}$, considering a density of $N_d = 1.0 \times 10^{16}\,\mathrm{cm}^{-3}$ with P atoms, and the ionization energy of shallow impurity $E_C - E_d = 0.045\,\mathrm{eV}$, with these values, a relative number of electrons in the donor state of less than $1\,\%$ is obtained. This example shows that at room temperature a small fraction of the electrons remains in the donor state, that is, practically all of them have passed to the conduction band.

To determine the electrostatic potential of interaction between electrons and ions, Poisson's equation is calculated with the corresponding charge density. This charge density generates a Hartree potential that modifies the bottom profile of the conduction band, to find the correct potential, states, energies, etc., the problem is approached by means of the self-consistent formalism, which is detailed in the next section.

It is interesting to take as a point of reference the previous work by Dakhlaoui *et al.* [7] of 2023 (previously mentioned in the introduction) as a comparison with the present work. In Dakhlaoui's work, some optical properties are calculated in Manning-like AlGaAs/GaAs double quantum Wells heterostructures (it should be noted that this type of potential is used to represent the vibrational energies

of some diatomic molecules), studying the effects of donors impurities. In the present work, a single AlGaAs/GaAs quantum well is calculated that can be modified by the introduction of the doped delta layer. In both works, the wave functions for different donor densities and positions of the doped layers have been represented.
In Dakhlaoui's work, the increase in the donor density causes a redshift in the optical absorption peaks caused by the approach between the corresponding states when the doped layer is located in the structure center of symmetry. In the present work, an opposite effect is presented, since when the donors' density increases, the quantum well depth, also increases and therefore the confined states separate (as will be seen later in the results and discussion section) and as a consequence of this, the absorption peaks present a blueshift.
Another interesting and practical work for comparisons was developed by Shao *et al.* [8] in 2006, in which the product of electron density and electron mobility was theoretically characterized by different variations in the system such as temperature and donor density for a single AlInSb/InSb quantum well system with a delta layer outside the well. As in the present work, a quantum well with a doped delta layer has also been analyzed, in the mentioned paper the change in the donor density was also characterized, however, an additional advantage of the present research work is the position characterization of the delta doped layer along the growth direction of the heterostructure, this is a significant change as it allows the possibility of going from a single quantum well to two coupled quantum wells (one caused by the band-offset between the materials and the other by the introduction of the delta layer). This difference significantly changes the optical properties of the system, which is an analysis that has been carried out in this work and was not studied in the aforementioned paper.

2.1. Optical absorption theory

The developments presented in this section are based on the original works of Ahn and Chuang from 1987 [9]. It is worth mentioning some pioneering works in these theoretical developments, such as Stern's in 1963 [10] and Kan *et al.* in 1987 [11]. Consider a two-level system with $|0\rangle$ and $|1\rangle$ (in coordinate representation, corresponds to Ψ_0 and Ψ_1 respectively, see Figure **2-2**) corresponding

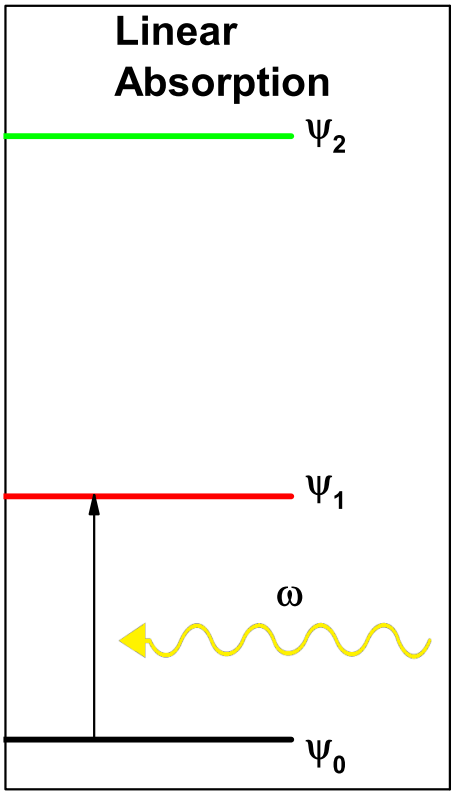

Figure 2-2.: Absorption diagram of a photon of frequency ω between states Ψ_0 and Ψ_1.

to the low and high level, respectively, in a monochromatic electromagnetic radiation presence of frequency ω (classic field), which is a coupling field with these states. The most common approach to tackle the problem of interaction of radiation with matter is that of the density matrix, whose time evolution is governed by the Liouville-Von Neumann equation (including dissipation terms):

$$\frac{\partial \rho}{\partial t} = \frac{1}{i\hbar}\left[H_0 - ME(t), \rho\right] - \frac{1}{2}\left[\gamma(\rho - \rho^{(0)}) + (\rho - \rho^{(0)})\gamma\right], \tag{2-5}$$

where ρ is the density matrix, H_0 is unperturbed Hamiltonian of the system, i.e. without the resonant electromagnetic radiation, M is a dipole operator, $E(t)$ the electric field with frequency ω, $\rho^{(0)}$ is the density matrix for the unperturbed system, and γ is the phenomenological term that accounts for the dissipation in the system presented by the presence of impurities or electron-phonon and

electron-electron interactions. γ can be considered as a diagonal matrix and its elements γ_{mm} correspond to the inverse of relaxation time for the $|m\rangle$ state. Defining the states $|a\rangle \equiv |0, k_y, k_z\rangle$ and $|b\rangle \equiv \left|1, k'_y, k'_z\right\rangle$, where 0 and 1 correspond to the states in the confinement direction or growth of the structure (x). The Hamiltonian H_0 has the eigenvalues E_a and E_b corresponding to the levels $|a\rangle$ and $|b\rangle$, respectively. These energies are given by:

$$E_a = E_0 + \frac{\hbar^2}{2m^*}\,(k_y^2 + k_z^2), \tag{2-6}$$

and

$$E_b = E_1 + \frac{\hbar^2}{2m^*}\,(k_y'^2 + k_z'^2), \tag{2-7}$$

where k_y and k_z are the wave vectors of the electron in the y and z directions. The electric field can be expressed as:

$$E(t) = Re\left(\mathcal{E}\, e^{-i\omega t}\right) = \frac{1}{2}\mathcal{E}\, e^{-i\omega t} + \frac{1}{2}\mathcal{E}\, e^{i\omega t} = \widetilde{E}\, e^{-i\omega t} + \widetilde{E}\, e^{i\omega t}, \tag{2-8}$$

where $\mathcal{E}$ denotes the amplitude of the field. The only nonzero matrix elements for the γ operator are:

$$\langle b|\gamma|b\rangle = \gamma_{bb} = \frac{1}{\tau_b} \quad \text{and} \quad \langle a|\gamma|a\rangle = \gamma_{aa} = \frac{1}{\tau_a}, \tag{2-9}$$

where τ_a and τ_b are the relaxation times for the states $|a\rangle$ and $|b\rangle$, respectively. One way to calculate the density matrix is by means of a perturbative method, expanding it in a power series as:

$$\rho = \sum_n \rho^{(n)}, \tag{2-10}$$

the density matrix for zero order $\rho^{(0)}$ has only diagonal elements because the electronic population is located in each of the states and there are no interaction effects between them. The notations used for the n-order density matrix elements are: $\rho_{aa}^{(n)} = \langle a|\rho^{(n)}|a\rangle$, $\rho_{ab}^{(n)} = \langle a|\,\rho^{(n)}\,|b\rangle$, $\rho_{ba}^{(n)} = \langle b|\,\rho^{(n)}\,|a\rangle$, and $\rho_{bb}^{(n)} = \langle b|\rho^{(n)}|b\rangle$. Thus, ρ has the symmetric property $\rho_{ab}(t) = \rho_{ab}^*(t)$.

By expanding the commutator from equation (2-5):

$$\begin{aligned}\frac{\partial\rho}{\partial t} = \frac{1}{i\hbar}\left[(H_0 - ME(t))\rho - \rho(H_0 - ME(t))\right] \\ - \frac{1}{2}\left[\gamma(\rho - \rho^{(0)}) + (\rho - \rho^{(0)})\gamma\right],\end{aligned} \tag{2-11}$$

by substituting (2-10) into equation (2-11):

$$\begin{aligned}\sum_n \frac{\partial\rho^{(n)}}{\partial t} = \frac{1}{i\hbar}\left[(H_0 - ME(t))\sum_n \rho^{(n)} - \sum_n \rho^{(n)}(H_0 - ME(t))\right] \\ - \frac{1}{2}\left[\gamma\left(\sum_n \rho^{(n)} - \rho^{(0)}\right) + \left(\sum_n \rho^{(n)} - \rho^{(0)}\right)\gamma\right],\end{aligned} \tag{2-12}$$

and taking into account that

$$\sum_n \rho^{(n)} - \rho^{(0)} = \left(\rho^{(0)} + \rho^{(1)} + \rho^{(2)} + ...\right) - \rho^{(0)} = \rho^{(1)} + \rho^{(2)} + \rho^{(3)} + ... = \sum_n \rho^{(n+1)}, \tag{2-13}$$

this expression is substituted into equation (2-12)

$$\begin{aligned}\sum_n \frac{\partial\rho^{(n)}}{\partial t} = \frac{1}{i\hbar}\left[(H_0 - ME(t))\sum_n \rho^{(n)} - \sum_n \rho^{(n)}(H_0 - ME(t))\right] \\ - \frac{1}{2}\left[\gamma\sum_n \rho^{(n+1)} + \sum_n \rho^{(n+1)}\gamma\right].\end{aligned} \tag{2-14}$$

For the calculation of the first order absorption, it is sufficient to calculate the matrix element ρ_{ba}. Applying the states $\langle b|$ and $|a\rangle$ on the left and right in the last equation, we obtain

$$\begin{aligned}\left\langle b\middle|\sum_n \frac{\partial\rho^{(n)}}{\partial t}\middle|a\right\rangle = \frac{1}{i\hbar}\left\langle b\middle|\sum_n \Big((H_0 - ME(t))\,\rho^{(n)} - \rho^{(n)}(H_0 - ME(t))\Big)\middle|a\right\rangle \\ - \frac{1}{2}\left\langle b\middle|\gamma\sum_n \rho^{(n+1)} + \sum_n \rho^{(n+1)}\gamma\middle|a\right\rangle,\end{aligned} \tag{2-15}$$

by using the distributing property:

$$\sum_n \frac{\partial}{\partial t}\left\langle b\middle|\rho^{(n)}\middle|a\right\rangle = \frac{1}{i\hbar}\sum_n\Bigg(\Big(\Big\langle b\Big|H_0\rho^{(n)}\Big|a\Big\rangle - \Big\langle b\Big|ME(t)\rho^{(n)}\Big|a\Big\rangle\Big) - \Big(\Big\langle b\Big|\rho^{(n)}H_0\Big|a\Big\rangle - \Big\langle b\Big|\rho^{(n)}ME(t)\Big|a\Big\rangle\Big)\Bigg) - \frac{1}{2}\Bigg(\sum_n\Big\langle b\Big|\gamma\rho^{(n+1)}\Big|a\Big\rangle + \sum_n\Big\langle b\Big|\rho^{(n+1)}\gamma\Big|a\Big\rangle\Bigg), \tag{2-16}$$

by using the completeness relation $|a\rangle\langle a| + |b\rangle\langle b| = \widehat{1}$ and substituting the corresponding energy values

$$\sum_n \frac{\partial}{\partial t}\left\langle b\middle|\rho^{(n)}\middle|a\right\rangle = \frac{1}{i\hbar}\sum_n\Bigg(\Big(E_b\rho_{ba}^{(n)} - \Big\langle b\Big|M(|a\rangle\langle a| + |b\rangle\langle b|)\rho^{(n)}\Big|a\Big\rangle E(t)\Big) - \Big(\rho_{ba}^{(n)}E_a - \Big\langle b\Big|\rho^{(n)}(|a\rangle\langle a| + |b\rangle\langle b|)M\Big|a\Big\rangle E(t)\Big)\Bigg) - \frac{1}{2}\Bigg(\sum_n\Big\langle b\Big|\gamma(|a\rangle\langle a| + |b\rangle\langle b|)\rho^{(n+1)}\Big|a\Big\rangle + \sum_n\Big\langle b\Big|\rho^{(n+1)}(|a\rangle\langle a| + |b\rangle\langle b|)\gamma\Big|a\Big\rangle\Bigg), \tag{2-17}$$

by distributing terms

$$\sum_n \frac{\partial\rho_{ba}^{(n)}}{\partial t} = \frac{1}{i\hbar}\sum_n\Bigg(E_b\rho_{ba}^{(n)} - \Big[\langle b|M|a\rangle\Big\langle a\Big|\rho^{(n)}\Big|a\Big\rangle + \langle b|M|b\rangle\Big\langle b\Big|\rho^{(n)}\Big|a\Big\rangle\Big]E(t) - \Big(\rho_{ba}^{(n)}E_a - \Big[\Big\langle b\Big|\rho^{(n)}\Big|a\Big\rangle\langle a|M|a\rangle + \Big\langle b\Big|\rho^{(n)}\Big|b\Big\rangle\langle b|M|a\rangle\Big]E(t)\Big)\Bigg) - \frac{1}{2}\Bigg(\sum_n\Big[\langle b|\gamma|a\rangle\Big\langle a\Big|\rho^{(n+1)}\Big|a\Big\rangle + \langle b|\gamma|b\rangle\Big\langle b\Big|\rho^{(n+1)}\Big|a\Big\rangle\Big] + \sum_n\Big[\Big\langle b\Big|\rho^{(n+1)}\Big|a\Big\rangle\langle a|\gamma|a\rangle + \Big\langle b\Big|\rho^{(n+1)}\Big|b\Big\rangle\langle b|\gamma|a\rangle\Big]\Bigg), \tag{2-18}$$

and taking into account that the matrix γ has only diagonal elements and by defining the matrix element of M as $M_{nm} \equiv \langle n|M|m\rangle$

$$\begin{aligned}\sum_n \frac{\partial \rho_{ba}^{(n)}}{\partial t} = \frac{1}{i\hbar}\sum_n \Bigg(& E_b \rho_{ba}^{(n)} - \left[M_{ba}\rho_{aa}^{(n)} + M_{bb}\rho_{ba}^{(n)}\right] E(t) \\ & - \left(\rho_{ba}^{(n)} E_a - \left[\rho_{ba}^{(n)} M_{aa} + \rho_{bb}^{(n)} M_{ba}\right] E(t)\right)\Bigg) \\ & - \frac{1}{2}\left(\sum_n \gamma_{bb}\rho_{ba}^{(n+1)} + \sum_n \rho_{ba}^{(n+1)}\gamma_{aa}\right),\end{aligned} \tag{2-19}$$

rewriting terms $E_{ba} = E_b - E_a$, $\Gamma_{ab} = \Gamma_{ba} = \frac{1}{2}\left(\frac{1}{\tau_a} + \frac{1}{\tau_b}\right)$, and reordering

$$\begin{aligned}\sum_n \frac{\partial \rho_{ba}^{(n)}}{\partial t} = \frac{1}{i\hbar}\sum_n \Bigg(& E_{ba}\rho_{ba}^{(n)} - \left(\rho_{aa}^{(n)} - \rho_{bb}^{(n)}\right) M_{ba}E(t) \\ & - \left(M_{bb} - M_{aa}\right)\rho_{ba}^{(n)} E(t)\Bigg) - \sum_n \Gamma_{ab}\rho_{ba}^{(n+1)},\end{aligned} \tag{2-20}$$

since the unperturbed density matrix only has diagonal elements, i.e. $\rho_{ba}^{(0)} = \rho_{ab}^{(0)} = 0$ which implies $\sum_n \rho_{ba}^{(n)} = \sum_n \rho_{ba}^{(n+1)}$, using this result in the last equation,

$$\begin{aligned}\sum_n \frac{\partial \rho_{ba}^{(n+1)}}{\partial t} = \frac{1}{i\hbar}\sum_n \Bigg(& E_{ba}\rho_{ba}^{(n+1)} - \left(\rho_{aa}^{(n)} - \rho_{bb}^{(n)}\right) M_{ba}E(t) \\ & - \left(M_{bb} - M_{aa}\right)\rho_{ba}^{(n)} E(t)\Bigg) - \sum_n \Gamma_{ab}\rho_{ba}^{(n+1)},\end{aligned} \tag{2-21}$$

extracting the nth term from this equation, it is possible to write a recurrence relation:

$$\begin{aligned}\frac{\partial \rho_{ba}^{(n+1)}}{\partial t} = & \left(\frac{1}{i\hbar}E_{ba} - \Gamma_{ab}\right)\rho_{ba}^{(n+1)} - \frac{1}{i\hbar}\left(\rho_{aa}^{(n)} - \rho_{bb}^{(n)}\right) M_{ba}E(t) \\ & - \frac{1}{i\hbar}\left(M_{bb} - M_{aa}\right) E(t)\rho_{ba}^{(n)},\end{aligned} \tag{2-22}$$

Expanding the density matrix elements as proportional terms of $e^{\pm i\omega t}$, it is possible to obtain the solutions for this equation by equaling both sides. Taking into account that there will be two equalities, one of them for the exponent sign (+) and the other one for (−). Under steady state conditions, the n-order perturbative term is:

$$\rho^{(n)}(t) = \tilde{\rho}^{(n)}(\omega)\, e^{-i\omega t} + \tilde{\rho}^{(n)}(-\omega)\, e^{i\omega t}, \tag{2-23}$$

which is valid for n odd.
Taking $n = 0$ in equation (2-22)

$$\frac{\partial \rho_{ba}^{(1)}}{\partial t} = \left(\frac{1}{i\hbar}E_{ba} - \Gamma_{ab}\right)\rho_{ba}^{(1)} - \frac{1}{i\hbar}\left(\rho_{aa}^{(0)} - \rho_{bb}^{(0)}\right) M_{ba}E(t). \tag{2-24}$$

Let $n = 1$ in equation (2-23) for the coupling $b - a$ and by substituting it in conjunction with equation (2-8) into equation (2-24)

$$\begin{aligned}
&\frac{\partial}{\partial t}\left(\tilde{\rho}_{ba}^{(1)}(\omega)\, e^{-i\omega t} + \tilde{\rho}_{ba}^{(1)}(-\omega)\, e^{i\omega t}\right) \\
&= \left(\frac{1}{i\hbar}E_{ba} - \Gamma_{ab}\right)\left(\tilde{\rho}_{ba}^{(1)}(\omega)\, e^{-i\omega t} + \tilde{\rho}_{ba}^{(1)}(-\omega)\, e^{i\omega t}\right) \\
&\quad - \frac{1}{i\hbar}\left(\rho_{aa}^{(n)} - \rho_{bb}^{(n)}\right) M_{ba}\left(\widetilde{E}\, e^{-i\omega t} + \widetilde{E}\, e^{i\omega t}\right),
\end{aligned} \tag{2-25}$$

evaluating the derivative and grouping the terms with negative and positive power,

$$\begin{aligned}
&-i\omega\tilde{\rho}_{ba}^{(1)}(\omega)\, e^{-i\omega t} + i\omega\tilde{\rho}_{ba}^{(1)}(-\omega)\, e^{i\omega t} \\
&= \left[\left(\frac{1}{i\hbar}E_{ba} - \Gamma_{ab}\right)\tilde{\rho}_{ba}^{(1)}(\omega) - \frac{1}{i\hbar}\left(\rho_{aa}^{(0)} - \rho_{bb}^{(0)}\right) M_{ba}\widetilde{E}\right] e^{-i\omega t} \\
&\quad + \left[\left(\frac{1}{i\hbar}E_{ba} - \Gamma_{ab}\right)\tilde{\rho}_{ba}^{(1)}(-\omega) - \frac{1}{i\hbar}\left(\rho_{aa}^{(0)} - \rho_{bb}^{(0)}\right) M_{ba}\widetilde{E}\right] e^{i\omega t},
\end{aligned} \tag{2-26}$$

equaling terms for the negative power and solving for $\rho_{ba}^{(1)}(\omega)$

$$\tilde{\rho}_{ba}^{(1)}(\omega) = \frac{\left(\rho_{aa}^{(0)} - \rho_{bb}^{(0)}\right) M_{ba}\widetilde{E}}{E_{ba} - \hbar\omega - i\hbar\Gamma_{ab}}, \tag{2-27}$$

where ρ_0 are the state occupations in equilibrium, and depend on the Fermi level of the system by means of the Fermi-Dirac distribution function,

$$\rho_{aa}^{(0)} = \frac{1}{1+e^{\beta\,(E_a - E_f)}} \quad \text{and} \quad \rho_{bb}^{(0)} = \frac{1}{1+e^{\beta\,(E_b - E_f)}}, \tag{2-28}$$

where E_f is the Fermi level of the system and $\beta = 1/k_B T$ is the Boltzmann factor, with T the temperature, and k_B the Boltzmann constant.
Remembering the relationship between the electronic polarization $P(t)$ and the susceptibility χ [12]:

$$P(t) = \varepsilon_0 \chi(\omega) \widetilde{E}\, e^{-i\omega t} + \varepsilon_0 \chi(-\omega) \widetilde{E}\, e^{i\omega t} = \frac{1}{V} Tr(\rho\, M), \tag{2-29}$$

where V is the volume, ε_0 is the vacuum permittivity. The absorption coefficient $\alpha(\omega)$ is related to χ by

$$\alpha(\omega) = \omega \sqrt{\frac{\mu}{\varepsilon_R}}\, \mathrm{Im}\left(\varepsilon_0 \chi(\omega)\right), \tag{2-30}$$

where μ is the permeability of the system, ε_R is the real part of the permittivity and $\chi(\omega)$ is the Fourier component of $\chi(t)$. The electronic polarization can be expressed as

$$P(t) = \frac{1}{V} \sum_{k_y,k_z} \sum_{k'_y,k'_z} \left[\langle a|\rho M|a\rangle + \langle b|\rho M|b\rangle\right], \tag{2-31}$$

where we can include the completeness relation:

$$P(t) = \frac{1}{V} \sum_{k_y,k_z} \sum_{k'_y,k'_z} \left[\langle a|\rho\left(|a\rangle\langle a| + |b\rangle\langle b|\right) M|a\rangle + \langle b|\rho\left(|a\rangle\langle a| + |b\rangle\langle b|\right) M|b\rangle\right], \tag{2-32}$$

by using distribute property

$$\begin{aligned} P(t) = \frac{1}{V} \sum_{k_y,k_z} \sum_{k'_y,k'_z} \big[& \langle a|\rho|a\rangle \langle a|M|a\rangle + \langle a|\rho|b\rangle \langle b|M|a\rangle \\ & + \langle b|\rho|a\rangle \langle a|M|b\rangle + \langle b|\rho|b\rangle \langle b|M|b\rangle \big], \end{aligned} \tag{2-33}$$

we can write this electronic polarization by using matrix notation and the definitions of ρ given by Eqs. (2-10) and (2-23)

$$P(t) = \frac{1}{V}\sum_{k_y,k_z}\sum_{k'_y,k'_z}\sum_{n}[\left(\tilde{\rho}^{(n)}_{aa}(\omega)M_{aa} + \tilde{\rho}^{(n)}_{ab}(\omega)M_{ba} + \tilde{\rho}^{(n)}_{ba}(\omega)M_{ab} + \tilde{\rho}^{(n)}_{bb}(\omega)M_{bb}\right)e^{-i\omega t} + \left(\tilde{\rho}^{(n)}_{aa}(-\omega)M_{aa} + \tilde{\rho}^{(n)}_{ab}(-\omega)M_{ba} + \tilde{\rho}^{(n)}_{ba}(-\omega)M_{ab} + \tilde{\rho}^{(n)}_{bb}(-\omega)M_{bb}\right)e^{i\omega t}], \tag{2-34}$$

for $n = 1$, and neglecting the terms outside of resonant transition $a - b$ and by using equation (2-29):

$$\varepsilon_0\chi^{(1)}(\omega)\widetilde{E} = \frac{1}{V}\sum_{k_y,k_z}\sum_{k'_y,k'_z}\left(2\tilde{\rho}^{(1)}_{ba}(\omega)M_{ab}\right), \tag{2-35}$$

by substituting equation (2-27) into equation (2-35). It follows that

$$\varepsilon_0\chi^{(1)}(\omega)\widetilde{E} = \frac{2}{V}\sum_{k_y,k_z}\sum_{k'_y,k'_z}\frac{\left(\rho^{(0)}_{aa} - \rho^{(0)}_{bb}\right)M_{ba}\widetilde{E}}{E_{ba} - \hbar\omega - i\hbar\Gamma_{ab}}M_{ab}, \tag{2-36}$$

deleting $\widetilde{E}$, remembering that $M_{ba} = M^*_{ab}$ and multiplying numerator and denominator by $E_{ba} - \hbar\omega + i\hbar\Gamma_{ba}$ in order to eliminate the imaginary number in denominator

$$\varepsilon_0\chi^{(1)}(\omega) = \frac{2}{V}\sum_{k_y,k_z}\sum_{k'_y,k'_z}\frac{\left(\rho^{(0)}_{aa} - \rho^{(0)}_{bb}\right)|M_{ab}|^2}{(E_{ba} - \hbar\omega - i\hbar\Gamma_{ab})}\frac{(E_{ba} - \hbar\omega + i\hbar\Gamma_{ab})}{(E_{ba} - \hbar\omega + i\hbar\Gamma_{ab})}, \tag{2-37}$$

this equation takes the form,

$$\varepsilon_0\chi^{(1)}(\omega) = \frac{2}{V}\sum_{k_y,k_z}\sum_{k'_y,k'_z}\left(\rho^{(0)}_{aa} - \rho^{(0)}_{bb}\right)|M_{ab}|^2\left(\frac{E_{ba} - \hbar\omega}{(E_{ba} - \hbar\omega)^2 + (\hbar\Gamma_{ab})^2} + i\frac{\hbar\Gamma_{ab}}{(E_{ba} - \hbar\omega)^2 + (\hbar\Gamma_{ab})^2}\right). \tag{2-38}$$

Hence, by substituting the imaginary part of this expression into equation (2-30), the absorption coefficient is finally obtained in linear order [9, 13]:

$$\alpha^{(1)}(\omega) = \omega \sqrt{\frac{\mu}{\varepsilon_R}} \sum_{k_y,k_z} \sum_{k'_y,k'_z} \frac{2}{V} \left(\rho^{(0)}_{aa} - \rho^{(0)}_{bb}\right) \frac{|M_{ab}|^2 \hbar \Gamma_{ab}}{(E_{ba} - \hbar\omega)^2 + (\hbar\Gamma_{ab})^2}\,, \tag{2-39}$$

the term M_{ab} is given by:

$$\begin{aligned} M_{ab} = e\,\langle a|\,x\,|b\rangle =& e\,\langle 0, k_y, k_z|\,x\,\left|1, k'_y, k'_z\right\rangle \\ &= e \int \Psi^*_0(x) x \Psi_1(x) dx\, \delta_{k_y,k'_y} \delta_{k_z,k'_z} = M_{01}\, \delta_{k_y,k'_y} \delta_{k_z,k'_z}\,, \end{aligned} \tag{2-40}$$

where δ_{k_j,k'_j} are Kronecker deltas, and

$$M_{01} \equiv e \int \Psi^*_1(x) x \Psi_2(x) dx\,. \tag{2-41}$$

replacing these results in 2-39, and writing the Γ_{01} in terms of the state relaxation time τ_0:

$$\alpha^{(1)}(\omega) = \omega \sqrt{\frac{\mu}{\varepsilon_R}} \sum_{k_y,k_z} \sum_{k'_y,k'_z} \frac{2}{V} \left(\rho^{(0)}_{aa} - \rho^{(0)}_{bb}\right) \frac{|M_{01}|^2 \hbar/\tau_0\, \delta_{k_y,k'_y} \delta_{k_z,k'_z}}{(E_{ba} - \hbar\omega)^2 + (\hbar/\tau_0)^2}\,, \tag{2-42}$$

evaluating the kronecker deltas with the sums:

$$\alpha^{(1)}(\omega) = \omega \sqrt{\frac{\mu}{\varepsilon_R}} \sum_{k_y,k_z} \frac{2}{V} \left(\rho^{(0)}_{aa} - \rho^{(0)}_{bb}\right) \frac{|M_{01}|^2 \hbar/\tau_0}{(E_{10} - \hbar\omega)^2 + (\hbar/\tau_0)^2}\,. \tag{2-43}$$

In the last equation, $E_{ba} = E_{10}$ has been used (for $k_y = k'_y$, and $k_z = k'_z$), according to the 2-6 and 2-7 equations. Defining $E_{10} \equiv \Delta E$, and $\varepsilon_R = \epsilon\,\epsilon_0$,

$$\alpha^{(1)}(\omega) = \omega \sqrt{\frac{\mu}{\epsilon\,\epsilon_0}} \sum_{k_y,k_z} \frac{2}{V} \left(\rho^{(0)}_{aa} - \rho^{(0)}_{bb}\right) \frac{|M_{01}|^2 \hbar/\tau_0}{(\Delta E - \hbar\omega)^2 + (\hbar/\tau_0)^2}\,. \tag{2-44}$$

The summation in 2-44 can be computed explicitly using 2-28:

$$\frac{2}{V} \sum_{k_y,k_z} \left(\rho^{(0)}_{aa} - \rho^{(0)}_{bb}\right) = \frac{2}{V} \sum_{k_y,k_z} \frac{1}{1 + e^{\beta\,(E_a - E_f)}} - \frac{2}{V} \sum_{k_y,k_z} \frac{1}{1 + e^{\beta\,(E_b - E_f)}}\,. \tag{2-45}$$

Let's calculate the first term on the right-hand side (the calculation of the second term is equivalent):

$$\frac{2}{V}\sum_{k_y,k_z}\frac{1}{1+e^{\beta\,(E_a-E_f)}}=\frac{2L_yL_z}{(2\pi)^2V}\int_0^\infty\int_0^\infty\frac{dk_yk_z}{1+e^{\beta\,(E_0+\vartheta(k_y^2+k_z^2)-E_f)}}\ , \tag{2-46}$$

in the last equation, the sums have been changed to integrals $\sum_{k_j}\{\cdots\}\rightarrow L_j/(2\pi)\int\{\cdots\}dk_j$ and 2-6 has been used with $\vartheta\equiv\hbar^2/(2m^*)$, where $j=y,z$ and L_j is the length of the system in the j direction. This integral can be evaluated using the change of variable to polar coordinates: $k_y=r\sin(\theta)$, $k_z=r\cos(\theta)$, and $dk_ydk_z=rdrd\theta$:

$$\frac{2}{V}\sum_{k_y,k_z}\frac{1}{1+e^{\beta\,(E_a-E_f)}}=\frac{2L_yL_z}{(2\pi)^2V}\int_0^{2\pi}d\theta\int_0^\infty\frac{rdr}{1+e^{\beta\,(\vartheta r^2+E_0-E_f)}}\ , \tag{2-47}$$

the volume of the system is given by $V=LS$, where S is the cross-sectional area of the structure which is given by $S=L_yL_z$, and L is the length of the quantum well then it remains:

$$\frac{2}{V}\sum_{k_y,k_z}\frac{1}{1+e^{\beta\,(E_a-E_f)}}=\frac{2}{2\pi L}\int_0^\infty\frac{rdr}{1+e^{\beta\,(\vartheta r^2+E_0-E_f)}}\ , \tag{2-48}$$

this expression can be rewritten as:

$$\frac{2}{V}\sum_{k_y,k_z}\frac{1}{1+e^{\beta\,(E_a-E_f)}}=\frac{1}{2\pi L}\frac{1}{\beta\vartheta}\int_0^\infty\frac{2\beta\vartheta rdr}{1+e^{\beta\,(\vartheta r^2+E_0-E_f)}}\ , \tag{2-49}$$

with $\varrho\equiv\beta(E_f-E_0)$, and changing variable $u=\beta\vartheta r^2$, then $du=2\beta\vartheta rdr$:

$$\frac{2}{V}\sum_{k_y,k_z}\frac{1}{1+e^{\beta\,(E_a-E_f)}}=\frac{1}{2\pi L}\frac{1}{\beta\vartheta}\int_0^\infty\frac{du}{1+e^{u-\varrho}}\ , \tag{2-50}$$

writing β and ϑ explicitly and evaluating the integral, we get

$$\frac{2}{V}\sum_{k_y,k_z}\frac{1}{1+e^{\beta\,(E_a-E_f)}}=\frac{2m^*k_BT}{2\pi\hbar^2L}\ln\left[1+e^{\varrho}\right]\ , \tag{2-51}$$

finally,

$$\frac{2}{V}\sum_{k_y,k_z}\frac{1}{1+e^{\beta\,(E_a-E_f)}}=\frac{m^*k_BT}{\pi\hbar^2L}\ln\left[1+\exp\left(\frac{E_f-E_0}{k_BT}\right)\right]\,. \tag{2-52}$$

This expression gives the number of electrons per unit volume with energy E_0 [4]. Equivalently, the second term on the right hand side in equation 2-45 is obtained:

$$\frac{2}{V}\sum_{k_y,k_z}\frac{1}{1+e^{\beta\,(E_b-E_f)}}=\frac{m^*k_BT}{\pi\hbar^2L}\ln\left[1+\exp\left(\frac{E_f-E_1}{k_BT}\right)\right]\,. \tag{2-53}$$

Now replacing 2-52 and 2-53 in 2-45:

$$\frac{2}{V}\sum_{k_y,k_z}\left(\rho_{aa}^{(0)}-\rho_{bb}^{(0)}\right)=\frac{m^*k_BT}{\pi\hbar^2L}\ln\left[\frac{1+\exp\left((E_f-E_0)/(k_BT)\right)}{1+\exp\left((E_f-E_1)/(k_BT)\right)}\right]\equiv\sigma_{01}\,. \tag{2-54}$$

This expression corresponds to the three-dimensional electronic concentration. Finally, replacing 2-54 in 2-44, the linear optical absorption coefficient is obtained [5, 9]:

$$\alpha^{(1)}(\omega)=\omega\sqrt{\frac{\mu}{\epsilon\,\epsilon_0}}\,\frac{|M_{01}|^2\sigma_{01}\hbar/\tau_0}{(\Delta E-\hbar\omega)^2+(\hbar/\tau_0)^2}\,. \tag{2-55}$$

2.2. Self-Consistent method

The self-consistent method [6, 14, 15] is a particularly useful method for calculating wave functions, energy levels, charge densities, electron density and Fermi level in systems that have regions with a certain donor density (acceptor density), that is, doped systems. This method takes into account the disturbance in the system generated by the electrostatic potential due to the donor's density, this term must be included in the Hamiltonian in a small percentage since, if 100 % of this disturbance is included, the convergence will not be reached.

According to Figure **2-1**, we define a confinement potential that accounts for the magnitude of the confinement potentials and the sizes of the structure. Let us define the electron confinement potential as

$$\mathcal{V}_c(x) \equiv \begin{cases} V_0\,, & \text{if } |x| > L/2 \\ 0\,, & \text{if } |x| \leq L/2\,. \end{cases} \tag{2-56}$$

The starting point of the self-consistent method is to solve the time independent Schrödinger equation considering only the electronic confinement potential, that is, the term $\mathcal{V}^{(0)}(x) \equiv \mathcal{V}_c(x)$,

$$-\frac{\hbar^2}{2\,m^*}\frac{\partial^2\psi_j^{(0)}(x)}{\partial x^2} + \mathcal{V}^{(0)}(x)\psi_j^{(0)}(x) = E_j^{(0)}\psi_j^{(0)}(x)\,. \tag{2-57}$$

In this equation, $\hbar$ corresponds to the reduced Planck constant, m^* is the effective mass which is taken equal in the region of wells and barriers, $\psi_j^{(0)}(x)$ is the wave function of the system corresponding to the eigenvalue $E_j^{(0)}$ (j corresponds to the j-th state, and the subscript (0) indicates the initial step in the self-consistent method).

Equation (2-57) can be solved using any numerical method; in particular, in this work, FDM [16, 17] will be used to solve all the equations involved in the problem (this method will be explained in the next section). Once The equation (2-57) is solved, a set of eigenfunctions and their corresponding eigenvalues, $\{\psi_j^{(0)}(x), E_j^{(0)}\}$, are obtained. On the other hand, the delta layer must contain a volumetric donor's density, n_d (electrons per cubic meter), additionally, the complete system must comply with the charge neutrality condition, which consists in that the total number of electrons per unit area must be equal to the number of ionized donors per unit area, that is, the following relationship must be met:

$$n_d\,\delta = \sum_j \frac{m^*\,k_B\,T}{\pi\,\hbar^2}\ln\left[1+\exp\left(\frac{E_f^{(0)}-E_j^{(0)}}{k_B\,T}\right)\right]\,, \tag{2-58}$$

where δ is the width of the delta doped layer, k_B is the Boltzmann constant, T is the system temperature (300 K in this work), $E_f^{(0)}$ is the Fermi level, and

$E_j^{(0)}$ are the eigenvalues obtained by means of equation (2-57). In the previous section, an equation for the number of electrons per unit of volume with a certain energy was demonstrated (equation 2-52), multiplying this equation by L and adding over all the states, the total number of electrons per unit area is obtained that corresponds to the right hand side in the equation 2-58. In equation (2-58), the only unknown term is the Fermi level, $E_f^{(0)}$. Clearly, this expression corresponds to a transcendental equation that can be solved for $E_f^{(0)}$. From the above, it follows that the second step in the self-consistent procedure is to use the charge neutrality relation to calculate the Fermi level.

Once the wave functions are calculated, the corresponding eigenvalues and the Fermi level in the system are obtained, from these, an expression for the electron density associated with the occupation of each of the states is obtained,

$$n^{(0)}(x) = \sum_j \frac{m^* k_B T}{\pi \hbar^2} \ln\left[1 + \exp\left(\frac{E_f^{(0)} - E_j^{(0)}}{k_B T}\right)\right] |\psi_j^{(0)}(x)|^2 . \tag{2-59}$$

The next step is to calculate the electrostatic potential, this procedure can be carried out by solving Poisson's equation considering a charge density associated with the ionized donors and the electron density,

$$\frac{d^2 \mathcal{V}_H^{(0)}(x)}{dx^2} = \frac{e^2}{\epsilon\, \epsilon_0}\left(n_d(x) - n^{(0)}(x)\right) , \tag{2-60}$$

where $\mathcal{V}_H^{(0)}(x)$ is the Hartree potential obtained in the first self-consistency step, e is the electron charge, ϵ_0 is the vacuum dielectric permittivity, and ϵ is the materials relative permittivity (which has been assumed to be constant in the whole heterostructure). Note that in equation (2-60), full ionization is being considered; this is a reasonable assumption for this material at room temperature. The function $n_d(x)$ takes the value of n_d in the region where the doped delta layer is located and is equal to zero at the other x-points. From the above, we can define a new electronic potential starting from the initial potential $\mathcal{V}^{(0)}(x) = \mathcal{V}_c(x)$, in the form $\mathcal{V}^{(1)}(x) = 95\,\%\mathcal{V}^{(0)}(x) + 5\,\%\left[\mathcal{V}_c(x) - \mathcal{V}_H^{(0)}(x)\right]$,

that is, 5 % of the Hartree disturbance potential has been included (the 5 % value has been chosen to guarantee that a significantly large perturbation in the electronic confinement potential that could lead to a numerical divergence is not generated. The chosen value, despite increasing the computational time, guarantees a correct convergence). With this potential, we can solve the Schrödinger equation again,

$$-\frac{\hbar^2}{2\,m^*}\frac{\partial^2\psi_j^{(1)}(x)}{\partial x^2}+\mathcal{V}^{(1)}(x)\psi_j^{(1)}(x)=E_j^{(1)}\psi_j^{(1)}(x)\,. \tag{2-61}$$

Through the solution of equation (2-61), a new set of eigenfunctions and eigenvalues $\{\psi_j^{(1)}(x), E_j^{(1)}\}$ is obtained to repeat the procedure again. In general, in an m-th step, it will be necessary to solve the Schrödinger equation:

$$-\frac{\hbar^2}{2\,m^*}\frac{\partial^2\psi_j^{(m)}(x)}{\partial x^2}+\mathcal{V}^{(m)}(x)\psi_j^{(m)}(x)=E_j^{(m)}\psi_j^{(m)}(x)\,. \tag{2-62}$$

In this equation the self-consistent potential has the form,

$$\mathcal{V}^{(m)}(x)=95\,\%\mathcal{V}^{(m-1)}(x)+5\,\%\left[\mathcal{V}_c(x)-\mathcal{V}_H^{(m-1)}(x)\right]\,, \tag{2-63}$$

where the Hartree potential $\mathcal{V}_H^{(m-1)}(x)$ is obtained by solving the equation:

$$\frac{d^2\mathcal{V}_H^{(m-1)}(x)}{dx^2}=\frac{e^2}{\epsilon\,\epsilon_0}\left(n_d(x)-n^{(m-1)}(x)\right) \tag{2-64}$$

with

$$n^{(m-1)}(x)=\quad\sum_j\frac{m^*\,k_B\,T}{\pi\,\hbar^2}\ln\left[1+\exp\left(\frac{E_f^{(m-1)}-E_j^{(m-1)}}{k_B\,T}\right)\right]\,|\,\psi_j^{(m-1)}(x)|^2\,. \tag{2-65}$$

In this equation, the Fermi level associated with the $m-1$ self-consistent step is calculated again using the charge neutrality condition,

$$n_d\,\delta=\sum_j\frac{m^*\,k_B\,T}{\pi\,\hbar^2}\ln\left[1+\exp\left(\frac{E_f^{(m-1)}-E_j^{(m-1)}}{k_B\,T}\right)\right]\,. \tag{2-66}$$

The parameter used to verify the convergence is the Fermi level E_f (in a completely analogous way, the wave function, the energies, etc. could be used). In this way, in each cycle of the procedure, the quantity $|E_f^{(m)} - E_f^{(m-1)}|$ is calculated. If in an N-th step this expression is less than a certain tolerance (for this work a value of 10^{-5} eV is sufficient), then the self-consistent process stops and the set of solutions found in this last step $\{\psi_j^{(N)}(x), \mathcal{V}^{(N)}(x), E_j^{(N)}, E_f^{(N)}, \mathcal{V}_H^{(N)}(x), n^{(N)}(x)\}$ must correspond to the self-consistent solution of the problem.

Figure **2-3** presents a block diagram that summarizes the self-consistent procedure as follows: starting from the solution of the Schrödinger equation with the potential $\mathcal{V}^{(0)}(x) \equiv \mathcal{V}_c(x)$; from the calculated eigenstates and eigenvalues, the charge neutrality is used to determine the Fermi level, with this Fermi level and the eigenstates, the electron density is constructed; from this density and considering the charge contribution generated by the doped delta layer, a charge density is defined that enters into Poisson's equation to obtain the Hartree potential. With this Hartree potential a new electronic potential is built and the Schrödinger equation is solved again with this new potential. At this point, a new set of eigenstates and eigenvalues is obtained, which are used again to calculate a new Fermi level through charge neutrality. Finally, the Fermi level is compared in this step with that obtained in the previous step. If a value less than a certain previously defined tolerance is obtained, the procedure is stopped; if on the contrary, a value greater than the tolerance is obtained, repeat the process until convergence is obtained.

2.3. Electromagnetically induced transparency (EIT)

EIT is an effect in which a material that presents high absorption at a certain wavelength between two states (Ψ_0 and Ψ_1) becomes transparent for that wavelength by taking advantage of the system interaction with two electromagnetic fields that are coupled to three levels in the system; these fields are normally known as probe field with a frequency of ω_p and control field with a frequency of ω_c [18, 19]. Early works in this field include Harris *et al.* from 1990 [20] and

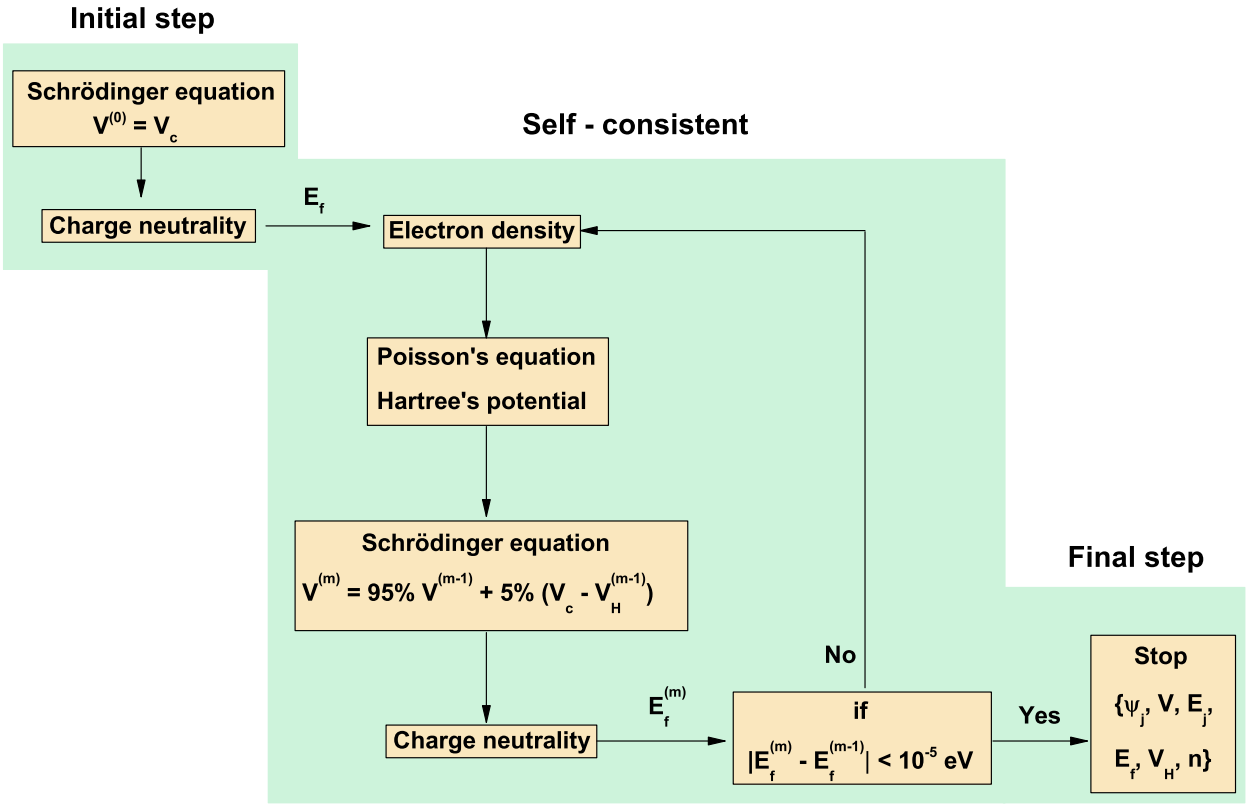

Figure 2-3.: Block diagram corresponding to the self-consistent algorithm.

Armstrong and Wynne from 1974 [21].
The probe field is associated with the coupling of the photons to the $\Psi_0 \rightarrow \Psi_1$ electronic transition. By considering only the probe field, it would generate an absorption peak located near the $E_1 - E_0$ energy transition. On the other hand, the control field refers to the coupling of the photons to the transition $\Psi_1 \rightarrow \Psi_2$. Depending on the characteristics of the control field, a destructive interference effect can be generated to attenuate the peak of maximum absorption mentioned above, making the system transparent for the energy in which it presented its maximum absorption.

This chapter is dedicated to the development of the expression for susceptibility considering the coupling between an atomic system modeled by a three-level system (three orthogonal states) with two external electromagnetic fields [22]. In Figure **2-4** the situation scheme is presented, where the ground state is characterized by the vector $|0\rangle$, the highest state as $|2\rangle$ and an intermediate state $|1\rangle$ (these states correspond to Ψ_0, Ψ_2 andΨ_1 respectively in coordinate representation), the system is immersed in two electromagnetic fields, a probe field of frequency ω_p that couples the states $|0\rangle$ with $|1\rangle$ and a control field of frequency ω_c that couple the states $|1\rangle$ and $|2\rangle$ (the coupling between the $|0\rangle$ and $|2\rangle$ state is dipolarly prohibited). The calculations are based on a semi-classical approach where the atomic system is a quantum system and the external fields are classical fields. In this development a cascade-type arrangement is considered, therefore, there is no strong dipolar coupling between $|0\rangle$ and $|2\rangle$.

For the phenomenon of EIT to occur, a three-level system (Ψ_0, Ψ_1, Ψ_2) is required with dipole coupling between Ψ_0, Ψ_1 and Ψ_1, Ψ_2 and forbidden coupling (or much smaller than those previously mentioned) between Ψ_0, Ψ_2, additionally, through the application of two electromagnetic fields (probe and control fields), a destructive quantum interference effect is generated between the two electronic transitions, resulting in the cancellation of optical absorption even in the presence of the applied field [22].

For absorption cancellation to occur, the system must initially be prepared with an electronic occupancy in the ground state and thus the imaginary part of the

susceptibility (at resonance) proportional to the atomic decay between Ψ_0, Ψ_2 (which is much less than 1 since it is a prohibited coupling) and since the imaginary part of the susceptibility is proportional to the optical absorption, then this is attenuated, giving rise to the EIT effect.

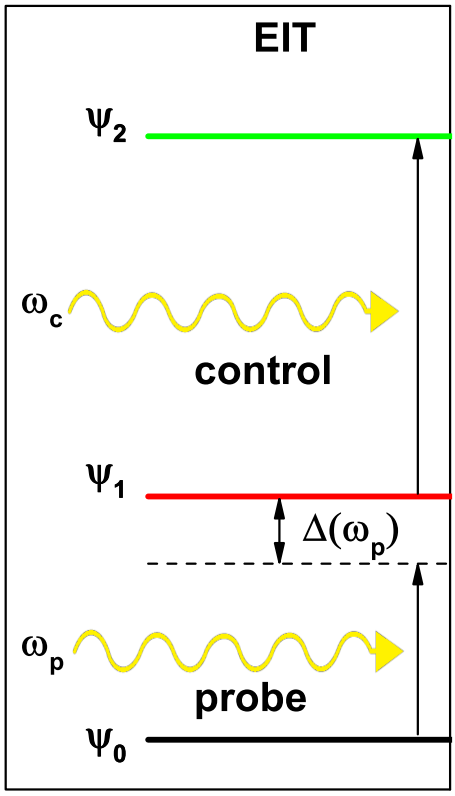

Figure 2-4.: Diagram of a three-level system (Ψ_0, Ψ_1, Ψ_2) in a cascade arrangement, interacting with two electromagnetic fields of frequencies ω_c and ω_p (control and probe respectively).

The detailed development of the theory is presented below.
The total Hamiltonian of the three level system is given by:

$$\widehat{H} = \widehat{H}_0 + \widehat{H}_1, \tag{2-67}$$

where $\widehat{H}_0$ is the Hamiltonian of the atomic system and $\widehat{H}_1$ represents the interaction of the atomic system with radiation. The three-level system corresponds

to a complete basis, therefore, it is possible to write the completex relation, $\widehat{I} = |1\rangle\langle 1| + |0\rangle\langle 0| + |2\rangle\langle 2|$, where $\widehat{I}$ is the identity operator in the base. Now, we can express the atomic system Hamiltonian using this left and right operator,

$$\widehat{H}_0 = \widehat{I}\widehat{H}_0\widehat{I}, \tag{2-68}$$

replacing the $\widehat{I}$ operator,

$$\widehat{H}_0 = (|1\rangle\langle 1| + |0\rangle\langle 0| + |2\rangle\langle 2|)\widehat{H}_0(|1\rangle\langle 1| + |0\rangle\langle 0| + |2\rangle\langle 2|), \tag{2-69}$$

making the products explicitly,

$$\widehat{H}_0 = |1\rangle\langle 1|\widehat{H}_0|1\rangle\langle 1|+|1\rangle\langle 1|\widehat{H}_0|0\rangle\langle 0|+|1\rangle\langle 1|\widehat{H}_0|2\rangle\langle 2|+|0\rangle\langle 0|\widehat{H}_0|1\rangle\langle 1|+|0\rangle\langle 0|\widehat{H}_0|0\rangle$$

$$\langle 0| + |0\rangle\langle 0|\widehat{H}_0|2\rangle\langle 2| + |2\rangle\langle 2|\widehat{H}_0|1\rangle\langle 1| + |2\rangle\langle 2|\widehat{H}_0|0\rangle\langle 0| + |2\rangle\langle 2|\widehat{H}_0|2\rangle\langle 2|,$$

the non-diagonal terms like $\langle 1|\widehat{H}_0|0\rangle$, $\langle 1|\widehat{H}_0|2\rangle$, $\langle 0|\widehat{H}_0|1\rangle$, $\langle 0|\widehat{H}_0|2\rangle$, $\langle 2|\widehat{H}_0|1\rangle$ and $\langle 2|\widehat{H}_0|0\rangle$ are canceled because the atomic system Hamiltonian corresponds to a diagonal matrix. On the other hand, since each state $|n\rangle$ corresponds to an eigenstate of the Hamiltonian $\widehat{H}_0$, then it is true that, $\widehat{H}_0|n\rangle = \hbar\omega_n|n\rangle$, with $n = 1, 0, 2$, where ω_n is the energy associated to the n state. The above result in the Hamiltonian associated to the atomic system with the form:

$$\widehat{H}_0 = \hbar\omega_1|1\rangle\langle 1| + \hbar\omega_0|0\rangle\langle 0| + \hbar\omega_2|2\rangle\langle 2|\,. \tag{2-70}$$

For the interaction Hamiltonian, we must take into account that there are two external fields in the system (probe and drive fields). In this case, we can consider that for both fields, the radiation is given with linear polarization in x, with this consideration, we can express the interaction Hamiltonian as follows:

$$\widehat{H}_1 = -e\,\widehat{x}\,E_p(t) - e\,\widehat{x}\,E_c(t), \tag{2-71}$$

where e is the electronic charge, $E_p(t)$ and $E_c(t)$ are the electric fields associated with the probe and control respectively. As with $\widehat{H}_0$, it is possible to act on the left and right with the identity operator to use the completex relation again,

$$\widehat{H}_1 = \widehat{I}\,\widehat{H}_1\,\widehat{I}, \tag{2-72}$$

replacing the $\widehat{I}$ operator, and by using the equation (2-71),

$$\widehat{H}_1 = (|1\rangle\langle 1| + |0\rangle\langle 0| + |2\rangle\langle 2|)\widehat{H}_1(|1\rangle\langle 1| + |0\rangle\langle 0| + |2\rangle\langle 2|)\,,$$

$$\widehat{H}_1 = -e(|1\rangle\langle 1| + |0\rangle\langle 0| + |2\rangle\langle 2|)\widehat{x}(|1\rangle\langle 1| + |0\rangle\langle 0| + |2\rangle\langle 2|)E_p(t)$$

$$-e(|1\rangle\langle 1| + |0\rangle\langle 0| + |2\rangle\langle 2|)\widehat{x}(|1\rangle\langle 1| + |0\rangle\langle 0| + |2\rangle\langle 2|)E_c(t)$$

It is clear that the terms $\langle 1|\widehat{x}|1\rangle$, $\langle 0|\widehat{x}|0\rangle$ and $\langle 2|\widehat{x}|2\rangle$ correspond to zero integrals due to the states symmetry, what's more, the $\langle 0|\widehat{x}|2\rangle$ and $\langle 2|\widehat{x}|0\rangle$ terms are zero because of the lambda arrangement, thus, we obtain the following expression:

$$\widehat{H}_1 = [-|1\rangle(e\langle 1|\widehat{x}|0\rangle)\langle 0| - |0\rangle(e\langle 0|\widehat{x}|1\rangle)\langle 1|]\,E_p(t)+$$

$$[-|1\rangle(e\langle 1|\widehat{x}|2\rangle)\langle 2| - |2\rangle(e\langle 2|\widehat{x}|1\rangle)\langle 1|]\,E_c(t)\,.$$

We can define the electric dipole matrix element as $M_{ij} = e\langle i|\widehat{x}|j\rangle = (e\langle i|\widehat{x}|j\rangle)^\dagger = (e\langle j|\widehat{x}|i\rangle)^* = M^*_{ji}$, with this definition, the last equation takes the form,

$$\widehat{H}_1 = -M_{10}\,E_p(t)\,|1\rangle\langle 0| - M_{12}\,E_c(t)\,|1\rangle\langle 2| + h.c.\,, \tag{2-73}$$

where $h.c.$ is the hermitian conjugate.
The equation 2-73 is still not the most convenient to use, an expression where the Rabi frequency is associated to the excited state and the intermediate state would be convenient. The fields $E_p(t)$ and $E_c(t)$ of equation (2-71) are classical fields, we can express them as follows: $E_p(t) = \mathcal{E}_p\cos(\omega_p t)$ and $E_c(t) = \mathcal{E}_c\cos(\omega_c t)$, where $\mathcal{E}_p$ and $\mathcal{E}_c$ are the amplitudes associated with the probe and control fields with frequencies ω_p and ν_c respectively. We can define ϕ_p and ϕ_c for the phases associated with the dipole operator matrix elements M_{10} and M_{12}, obtaining $M_{10} = |M_{10}|e^{-i\phi_p}$ and $M_{12} = |M_{12}|e^{-i\phi_c}$. In this way, we can define the Rabi frequency associated with each of the couplings:

$$\Omega_p = \frac{|M_{10}|\mathcal{E}_p}{\hbar} \quad \text{and} \quad \Omega_c = \frac{|M_{12}|\mathcal{E}_c}{\hbar}\,. \tag{2-74}$$

To obtain the equation of the dipole electric moment for the probe and control fields we can write M_{10} and M_{12} in terms of the Rabi frequency,

$$M_{10} = \frac{\hbar\Omega_p}{\mathcal{E}_p} e^{-i\phi_p} \quad \text{and} \quad M_{12} = \frac{\hbar\Omega_c}{\mathcal{E}_c} e^{-i\phi_c}\,, \tag{2-75}$$

it is convenient to rewrite the fields in their exponential form,

$$E_p(t) = \frac{\mathcal{E}_p}{2}(e^{-i\omega_p t} + e^{i\omega_p t}) \quad \text{and} \quad E_c(t) = \frac{\mathcal{E}_c}{2}(e^{-i\omega_c t} + e^{i\omega_c t})\,, \tag{2-76}$$

taking into account the Eqs. 2-75 and 2-76, we can express the term $M_{10}\,E(t)$ of equation (2-73) in a new form:

$$M_{10}\,E_p(t) = \frac{\hbar\Omega_p}{\mathcal{E}_p} e^{-i\phi_p} \cdot \frac{\mathcal{E}_p}{2}(e^{-i\omega_p t} + e^{i\omega_p t})\,,$$

$$M_{10}\,E_p(t) = \frac{\hbar\Omega_p}{2}(e^{-i\phi_p} e^{-i\omega_p t}) + \frac{\hbar\Omega_p}{2} e^{-i\phi_p} e^{i\omega_p t}\,,$$

The second term of the expression $M_{10}\,E(t)$ does not contribute significantly in the calculation of the electronic population, by using the rotating wave approximation we can see that the term is of high oscillations, then $M_{10}\,E(t)$ is written as follows:

$$M_{10}\,E_p(t) = \frac{\hbar\Omega_p}{2}\, e^{-i\phi_p} e^{-i\omega_p t}\,. \tag{2-77}$$

In the same way we calculate $M_{12}\,E_c(t)$,

$$M_{12}\,E_c(t) = \frac{\hbar\Omega_c}{2}\, e^{-i\phi_c} e^{-i\omega_c t}\,. \tag{2-78}$$

Replacing (2-77) and (2-78) in (2-73):

$$\widehat{H}_1 = -\left(\frac{\hbar\Omega_p}{2}\, e^{-i\phi_p} e^{-i\omega_p t}\right) |1\rangle\langle 0| - \left(\frac{\hbar\Omega_c}{2}\, e^{-i\phi_c} e^{-i\omega_c t}\right) |1\rangle\langle 2| + h.c.\,. \tag{2-79}$$

From equation 2-75 we obtain $\Omega_p e^{-i\phi_p} = M_{10}\mathcal{E}_p/\hbar$, replacing in equation (2-79) we obtain the interaction Hamiltonian between the system with the external fields $\widehat{H}_1$ in a explicit form in terms of the amplitude of the probe field $\mathcal{E}_p$, the associated dipole moment M_{10}, the external frequency ω_p and the Rabi frequency of the system Ω_c,

$$\widehat{H}_1 = -\frac{M_{10}}{2}\,\mathcal{E}_p e^{-i\omega_p t}\,|1\rangle\langle 0| - \frac{\hbar\Omega_c}{2}\,e^{-i\phi_c}e^{-i\omega_c t}\,|1\rangle\langle 2| + h.c.\,. \tag{2-80}$$

We can use the Von Neumann equation to analyze the time evolution by means of the density operator,

$$\frac{\partial\widehat{\rho}}{\partial t} = -\frac{i}{\hbar}\left[\widehat{H},\widehat{\rho}\right] - \frac{1}{2}\left\{\widehat{\Gamma},\widehat{\rho}\right\}, \tag{2-81}$$

we must take into account that $\left[\widehat{H},\widehat{\rho}\right]$ is a commutator and $\left\{\widehat{\Gamma},\widehat{\rho}\right\}$ is an anticonmutator. To calculate the matrix elements of this equation, we must expand the products and use the completex relation between operators, with an arbitrary matrix element the last equation can be written as,

$$\dot{\rho_{ij}} = -\frac{i}{\hbar}\sum_k(H_{ik}\rho_{kj} - \rho_{ik}H_{kj}) - \frac{1}{2}\sum_k(\Gamma_{ik}\rho_{kj} + \rho_{ik}\Gamma_{kj})\,, \tag{2-82}$$

the terms Γ_{kj} and Γ_{ik} are dissipative elements and can be expressed as $\Gamma_{nm} = \langle n|\widehat{\Gamma}|m\rangle = \Upsilon_n\delta_{nm}$ with $n, m = \{1, 0, 2\}$ where δ_{nm} is the Kronecker delta. From the above, we see that Γ is a diagonal matrix, secondly, the term Υ_n is inversely proportional to the state decay times, additionally, since states $|0\rangle$ and $|2\rangle$ are not dipolarly coupled, thus, the decay time for these states will be very high and consequently the Γ associate with the coupling between these states will be smaller.

To calculate the matrix element of ρ_{10} we make $i = 1$ and $j = 0$ in equation (2-82),

$$\dot{\rho_{10}} = -\frac{i}{\hbar}\sum_k(H_{1k}\rho_{k0} - \rho_{1k}H_{k0}) - \frac{1}{2}\sum_k(\Gamma_{1k}\rho_{k0} + \rho_{1k}\Gamma_{k0})\,, \tag{2-83}$$

$$\dot{\rho_{10}} = -\frac{i}{\hbar}[H_{11}\rho_{10} - \rho_{11}H_{10} + H_{10}\rho_{00} - \rho_{10}H_{00} + H_{12}\rho_{20} - \rho_{12}H_{20}]$$

$$-\frac{1}{2}[\Gamma_{11}\rho_{10} + \rho_{11}\Gamma_{10} + \Gamma_{10}\rho_{00} + \rho_{10}\Gamma_{00} + \Gamma_{12}\rho_{20} + \rho_{12}\Gamma_{20}]\,, \tag{2-84}$$

the non-diagonal terms of Γ have been canceled, at this point it is necessary to explicitly calculate the matrix elements associated with the complete Hamiltonian $\widehat{H}_0 + \widehat{H}_1$, this is easy to do by means of equations (2-70) and (2-80),

$$H_{11} = \langle 1|\widehat{H}_0|1\rangle + \langle 1|\widehat{H}_1|1\rangle = \hbar\omega_1\,, \tag{2-85}$$

$$H_{10} = \langle 1|\widehat{H}_0|0\rangle + \langle 1|\widehat{H}_1|0\rangle = -\frac{M_{10}\,\mathcal{E}_p}{2}\,e^{-i\omega_p t}\,, \tag{2-86}$$

$$H_{00} = \langle 0|\widehat{H}_0|0\rangle + \langle 0|\widehat{H}_1|0\rangle = \hbar\omega_0\,, \tag{2-87}$$

$$H_{12} = \langle 1|\widehat{H}_0|2\rangle + \langle 1|\widehat{H}_1|2\rangle = -\frac{\hbar\Omega_c}{2}\,e^{-i\phi_c}\,e^{-i\omega_c t}\,, \tag{2-88}$$

$$H_{20} = \langle 1|\widehat{H}_0|0\rangle + \langle 1|\widehat{H}_1|0\rangle = 0\,, \tag{2-89}$$

considering $\Gamma_{11} = \Gamma_{00} \equiv \gamma_{01}$ and replacing equations (2-85 - 2-89) in (2-84):

$$\dot{\rho_{10}} = -\frac{i}{\hbar}[\hbar\omega_1\,\rho_{10} + \frac{M_{10}\,\mathcal{E}_p}{2}\,e^{-i\omega_p t}\rho_{11} - \frac{M_{10}\,\mathcal{E}_p}{2}\,e^{-i\omega_p t}\rho_{00} - \hbar\omega_0\,\rho_{10}$$

$$-\frac{\hbar\Omega_c}{2}\,e^{-i\phi_c}\,e^{-i\omega_c t}\rho_{20}] - \frac{1}{2}[\gamma_{01}\rho_{10} + \gamma_{01}\,\rho_{10}]\,,$$

$$\dot{\rho_{10}} = -i\omega_1\,\rho_{10} + i\omega_0\,\rho_{10} - \frac{iM_{10}\,\mathcal{E}_p}{2\hbar}\,e^{-i\omega_p t}\,\rho_{11} + \frac{iM_{10}\,\mathcal{E}_p}{2\hbar}\,e^{-i\omega_p t}\,\rho_{00} +$$
$$\frac{i}{2}\Omega_c\,e^{-i\phi_c}\,e^{-i\omega_c t}\,\rho_{20} - \gamma_{01}\,\rho_{10}\,,$$

defining $\omega_{10} = \omega_1 - \omega_0$, a final equation is obtained for the matrix element ρ_{10},

$$\dot{\rho_{10}} = -(i\omega_{10} + \gamma_{01})\,\rho_{10} - \frac{iM_{10}\,\mathcal{E}_p}{2\hbar}\,e^{-i\omega_p t}(\rho_{11} - \rho_{00}) + \frac{i}{2}\Omega_c e^{-i\phi_c} e^{-\omega_c t}\rho_{20}\,. \quad (2\text{-}90)$$

In the same way, we can calculate the term $\dot{\rho_{20}}$ making $i = 2$ and $j = 0$ in equation (2-82),

$$\dot{\rho_{20}} = -\frac{i}{\hbar}\sum_k (H_{2k}\rho_{k0} - \rho_{2k}H_{k0}) - \frac{1}{2}\sum_k (\Gamma_{2k}\rho_{k0} + \rho_{2k}\Gamma_{k0})\,, \quad (2\text{-}91)$$

expanding the summation,

$$\dot{\rho_{20}} = -\frac{i}{2}[H_{21}\rho_{10} - \rho_{21}H_{10} + H_{20}\rho_{00} - \rho_{20}H_{00} + H_{22}\rho_{20} - \rho_{22}H_{20}] -$$

$$-\frac{1}{2}[\Gamma_{21}\rho_{10} + \rho_{21}\Gamma_{10} + \Gamma_{20}\rho_{00} + \rho_{20}\Gamma_{00} + \Gamma_{22}\rho_{20} + \rho_{22}\Gamma_{20}]\,, \quad (2\text{-}92)$$

once again the terms corresponding to non-diagonal Γ have been canceled. Following the same steps as in the calculation of ρ_{10}, the matrix elements are obtained,

$$H_{21} = -\frac{\hbar\,\Omega_c}{2}\,e^{i\phi_c}\,e^{i\omega_c t}\,, \quad (2\text{-}93)$$

$$H_{10} = -\frac{M_{10}\,\mathcal{E}_p}{2}\,e^{-i\omega_p t}\,, \quad (2\text{-}94)$$

$$H_{20} = 0\,, \quad (2\text{-}95)$$

$$H_{00} = \hbar\,\omega_0\,, \tag{2-96}$$

$$H_{22} = \hbar\,\omega_2\,, \tag{2-97}$$

considering $\Gamma_{00} = \Gamma_{22} \equiv \gamma_{02}$ taking into account that they are associated to the same transition, and replacing equations (2-93 - 2-97) in (2-92):

$$\dot{\rho_{20}} = -\frac{i}{\hbar}\left[-\frac{\hbar\,\Omega_c}{2}\,e^{i\phi_c}\,e^{i\omega_c t}\,\rho_{10} + \frac{M_{10}\,\mathcal{E}_p}{2}\,e^{-i\omega_p t}\,\rho_{21} - \hbar\omega_0\,\rho_{20} + \hbar\omega_2\,\rho_{20}\right] -$$

$$-\frac{1}{2}[\gamma_{02}\,\rho_{20} + \gamma_{02}\,\rho_{20}]\,. \tag{2-98}$$

It is pertinent to remember that γ_{02} will have a very small value because the time for electronic decay between these states will be very high, removing the parentheses in the last equation,

$$\dot{\rho_{20}} = i\omega_0\rho_{20} - i\omega_2\,\rho_{20} - \frac{iM_{10}\,\mathcal{E}_p}{2\hbar}\,e^{-i\omega_p t}\,\rho_{21} + \frac{i\Omega_c}{2}\,e^{i\phi_c}e^{i\omega_c t}\,\rho_{10} - \gamma_{02}\rho_{20}\,, \tag{2-99}$$

defining $\omega_{20} = \omega_2 - \omega_0$, and rearranging terms, it is finally obtained,

$$\dot{\rho_{20}} = -(i\omega_{20} + \gamma_{02})\,\rho_{20} - \frac{iM_{10}\,\mathcal{E}_p}{2\hbar}\,e^{-i\omega_p t}\,\rho_{21} + \frac{i\Omega_c}{2}\,e^{i\phi_c}e^{i\omega_c t}\,\rho_{10}\,. \tag{2-100}$$

Similarly, we can calculate the term $\dot{\rho_{12}}$ by doing $i = 1$ and $j = 2$ in the equation (2-82),

$$\dot{\rho_{12}} = -\frac{i}{\hbar}\sum_k (H_{1k}\rho_{k2} - \rho_{1k}H_{k2}) - \frac{1}{2}\sum_k (\Gamma_{1k}\rho_{k2} + \rho_{1k}\Gamma_{k2})\,, \tag{2-101}$$

expanding the summations,

$$\dot{\rho_{12}} = -\frac{i}{\hbar}[H_{11}\rho_{12} - \rho_{11}H_{12} + H_{10}\rho_{02} - \rho_{10}H_{02} + H_{12}\rho_{22} - \rho_{12}H_{22}]$$

$$-\frac{1}{2}[\Gamma_{11}\rho_{12} + \rho_{11}\Gamma_{12} + \Gamma_{10}\rho_{02} + \rho_{10}\Gamma_{02} + \Gamma_{12}\rho_{22} + \rho_{12}\Gamma_{22}]\,, \tag{2-102}$$

the procedure is similar to the one already presented, it is easy to see that the matrix elements have the form,

$$H_{11} = \hbar\,\omega_1\,, \tag{2-103}$$

$$H_{12} = -\frac{\hbar\,\Omega_c}{2}\,e^{-i\phi_c}\,e^{-i\omega_c t}\,, \tag{2-104}$$

$$H_{10} = -\frac{M_{10}\,\mathcal{E}_p}{2}\,e^{-i\omega_p t}\,, \tag{2-105}$$

$$H_{02} = 0\,, \tag{2-106}$$

$$H_{22} = \hbar\,\omega_2\,, \tag{2-107}$$

making $\Gamma_{11} = \Gamma_{22} \equiv \gamma_{12}$ and replacing the Eqs. (2-103 - 2-107) in equation (2-102),

$$\dot{\rho_{12}} = -\frac{i}{\hbar}\left[\hbar\omega_1\,\rho_{12} + \frac{\hbar\,\Omega_c}{2}\,e^{-i\phi_c}\,e^{-i\omega_c t}\,\rho_{11} - \frac{M_{10}\,\mathcal{E}_p}{2}\,e^{-i\omega_p t}\,\rho_{02} - \frac{\hbar\,\Omega_c}{2}\,e^{-i\phi_c}\,e^{-i\omega_c t}\,\rho_{22} - \hbar\omega_2\,\rho_{12}\right]$$

$$-\frac{1}{2}\left[\gamma_{12}\,\rho_{12} + \gamma_{12}\,\rho_{12}\right]\,, \tag{2-108}$$

defining $\omega_{12} = \omega_1 - \omega_2$ and regrouping, we finally obtain,

$$\dot{\rho_{12}} = -(i\omega_{12}+\gamma_{12})\,\rho_{12} - \frac{i}{2}\Omega_c\, e^{-i\phi_c}\, e^{-i\omega_c t}\,(\rho_{11}-\rho_{22}) + \frac{iM_{10}\,\mathcal{E}_p}{2\hbar}\, e^{-i\omega_p t}\,\rho_{02}\,. \quad (2\text{-}109)$$

The absorption in the system is proportional to the density matrix associated with the transition $|0\rangle \rightarrow |1\rangle$, ρ_{10}. We can consider as initial condition the system is in the ground state, this means that at time $t = 0$ all electronic population are in $|0\rangle$, this implies that $\rho_{00}^{(0)} = 1$ and in the state $|1\rangle$ and $|2\rangle$ we will have zero $\rho_{11}^{(0)} = \rho_{22}^{(0)} = 0$, remembering that the diagonal terms of the density matrix are associated with the probability density of each state. In the same way we can consider $\rho_{21}^{(0)} = 0$ which corresponds to the fact that there are no excitations in the system for $t = 0$. Let's make $\rho_{10} = \tilde{\rho}_{10}\, e^{i\omega_p t}$ and $\rho_{20} = \tilde{\rho}_{20}\, e^{-i(\omega_p+\omega_{21})t}$ where $\tilde{\rho}_{10}$ and $\tilde{\rho}_{20}$ have no time dependency. By evaluating in the equation (2-90),

$$-i\nu\,\tilde{\rho}_{10}\, e^{-i\omega_p t} = -(i\omega_{10}+\gamma_{01})\tilde{\rho}_{10}\, e^{-i\omega_p t} - \frac{iM_{10}\,\mathcal{E}_p}{2\hbar}(\rho_{11}-\rho_{00}) + \frac{i}{2}\Omega_c e^{-i\phi_c} e^{-i\omega_c t}\tilde{\rho}_{20}\, e^{-i(\omega_p+\omega_{21})t}\,, \quad (2\text{-}110)$$

with $t = 0$,

$$-i\nu\tilde{\rho}_{10} = -(i\omega_{10} + \gamma_{01})\tilde{\rho}_{10} - \frac{iM_{10}\,\mathcal{E}_p}{2\hbar}(\rho_{11}^{(0)} - \rho_{00}^{(0)}) + \frac{i}{2}\Omega_c e^{-i\phi_c}\tilde{\rho}_{20}\,,$$

reorganizing terms and applying the initial conditions for $\rho_{11}^{(0)}$ and $\rho_{00}^{(0)}$,

$$0 = -(\gamma_{01} + i(\omega_{10} - \omega_p))\,\tilde{\rho}_{10} + \frac{iM_{10}\,\mathcal{E}_p}{2\hbar} + \frac{i}{2}\Omega_c e^{-i\phi_c}\,\tilde{\rho}_{20}\,, \quad (2\text{-}111)$$

defining the detuning $\Delta(\omega_p) = \omega_{10} - \omega_p$ as the difference between the transition energy between $|0\rangle$ and $|1\rangle$ states and the energy of the probe field, we obtain

$$0 = -(\gamma_{01} + i\Delta)\tilde{\rho}_{10} + \frac{iM_{10}\,\mathcal{E}_p}{2\hbar} + \frac{i}{2}\Omega_c e^{-i\phi_c}\tilde{\rho}_{20}\,. \quad (2\text{-}112)$$

Secondly, by using the expressions $\rho_{10} = \tilde{\rho}_{10}\, e^{i\omega_p t}$ and $\rho_{20} = \tilde{\rho}_{20}\, e^{-i(\omega_p+\omega_{21})t}$ in the equation (2-100),

$$-i(\omega_p+\omega_{21})\tilde{\rho}_{20}\, e^{-i(\omega_p+\omega_{21})t} = -(i\omega_{20}+\gamma_{02})\,\tilde{\rho}_{20}\, e^{-i(\omega_p+\omega_{21})t} - \frac{iM_{10}\,\mathcal{E}_p}{2\hbar}\, e^{-i\omega_p t}\rho_{21}$$

$$+\frac{i}{2}\Omega_c\, e^{i\phi_c}\, e^{i\omega_c t}\tilde{\rho}_{10}\, e^{-i\omega_p t}\,,$$

evaluating for $t = 0$,

$$-i(\omega_p+\omega_{21})\,\tilde{\rho}_{20} = -(i\omega_{20}+\gamma_{02})\,\tilde{\rho}_{20} - \frac{iM_{20}\,\mathcal{E}_p}{2\hbar}\,\rho_{21}^{(0)} + \frac{i}{2}\Omega_c\, e^{i\phi_c}\,\tilde{\rho}_{10}\,, \tag{2-113}$$

rearranging terms,

$$0 = -(\gamma_{02} + i(\omega_{20}-\omega_{21}-\omega_p))\,\tilde{\rho}_{20} + \frac{i}{2}\Omega_c\, e^{i\phi_c}\,\tilde{\rho}_{10}\,, \tag{2-114}$$

let's see that,

$$\omega_{20}-\omega_{21} = \omega_2-\omega_0-\omega_2+\omega_1\,,$$

$$\omega_{20}-\omega_{21} = \omega_1-\omega_0\,,$$

$$\omega_{20}-\omega_{21} = \omega_{10}\,,$$

by using this result in (2-114), remembering the detuning definition,

$$0 = -(\gamma_{02} + i\Delta(\omega_p))\,\tilde{\rho}_{20} + \frac{i}{2}\Omega_c\, e^{i\phi_c}\,\tilde{\rho}_{10}\,. \tag{2-115}$$

From this last equation, let's solve for the term $\tilde{\rho}_{20}$,

$$\tilde{\rho}_{20} = \frac{i\Omega_c\, e^{i\phi_c}}{2\,(\gamma_{02}+i\Delta(\omega_p))}\,\tilde{\rho}_{10}\,, \tag{2-116}$$

replacing equation (2-116) in (2-112):

$$0 = -(\gamma_{01} + i\Delta(\omega_p))\,\tilde{\rho}_{10} + \frac{iM_{10}\,\mathcal{E}_p}{2\hbar} + \frac{i}{2}\Omega_c\,e^{-i\phi_c}\frac{i\Omega_c\,e^{i\phi_c}}{2\,(\gamma_{02} + i\Delta(\omega_p))}\,\tilde{\rho}_{10}\,,$$

simplifying,

$$0 = -(\gamma_{01} + i\Delta(\omega_p))\,\tilde{\rho_{10}} + \frac{iM_{10}\,\mathcal{E}_p}{2\hbar} - \frac{\Omega_c^2\,\tilde{\rho}_{10}}{4\,(\gamma_{02} + i\Delta(\omega_p))}\,,$$

solving for $\tilde{\rho}_{10}$,

$$\left[(\gamma_{01} + i\Delta(\omega_p)) + \frac{\Omega_c^2}{4\,(\gamma_{02} + i\Delta(\omega_p))}\right]\,\tilde{\rho}_{10} = \frac{iM_{10}\,\mathcal{E}_p}{2\hbar}\,,$$

$$\frac{4\,(\gamma_{01} + i\Delta(\omega_p))(\gamma_{02} + i\Delta(\omega_p)) + \Omega_c^2}{4\,(\gamma_{02} + i\Delta(\omega_p))}\,\tilde{\rho}_{10} = \frac{iM_{10}\,\mathcal{E}_p}{2\hbar}\,,$$

$$\tilde{\rho}_{10} = \frac{4\,iM_{10}\,\mathcal{E}_p\,(\gamma_{02} + i\Delta(\omega_p))}{2\hbar\,[4\,(\gamma_{01} + i\Delta(\omega_p))\,(\gamma_{02} + i\Delta(\omega_p)) + \Omega_c^2]}\,,$$

$$\tilde{\rho}_{10} = \frac{iM_{10}\,\mathcal{E}_p\,(\gamma_{02} + i\Delta(\omega_p))}{2\hbar\,[(\gamma_{01} + i\Delta(\omega_p))\,(\gamma_{02} + i\Delta(\omega_p)) + \Omega_c^2/4]}\,, \tag{2-117}$$

remembering that $\rho_{10} = \tilde{\rho}_{10}\,e^{-\omega_p t}$, then we finally get,

$$\rho_{10} = \frac{iM_{10}\,\mathcal{E}_p\,(\gamma_{02} + i\Delta(\omega_p))\,e^{-i\omega_p t}}{2\hbar[(\gamma_{01} + i\Delta(\omega_p))\,(\gamma_{02} + i\Delta(\omega_p)) + \Omega_c^2/4]}\,. \tag{2-118}$$

From the equation (2-76), it is had that by means of the rotating wave approximation only a part of the field contributes significantly to the electronic population between the levels $|0\rangle$ and $|1\rangle$, this part is given by $E_p(t) = \mathcal{E}_p\,e^{-i\omega_p t}/2$, in the same way, the macroscopic polarization will be given by $P_p(t) = \wp_p\,e^{-i\omega_p t}/2$, where $\wp_p$ is the complex polarization of the system. From the above, we can write complex polarization in terms of macroscopic polarization as,

$$\wp_p = 2\, P_p(t)\, e^{i\omega_p t}\,. \tag{2-119}$$

To obtain an expression for the polarization of the system due to the $|0\rangle \rightarrow |1\rangle$ transition, then the wave function of the system can be approximated as a linear combination of these states,

$$|\psi(t)\rangle = C_1(t)\,|1\rangle + C_0(t)\,|0\rangle\,, \tag{2-120}$$

on the other hand, the macroscopic polarization can be calculated as,

$$P_p(t) = e\,\langle\psi(t)|x|\psi(t)\rangle =$$

$$P_p(t) = e\,\left(C_1^*(t)\,\langle 1| + C_0^*(t)\,\langle 0|\right) x\,\left(C_1(t)\,|1\rangle + C_0(t)\,|0\rangle\right) =$$

$$P_p(t) = e\,C_1^*(t)C_0(t)\,\langle 1|x|0\rangle + e\,C_1(t)C_0^*(t)\,\langle 0|x|1\rangle =$$

$$P_p(t) = C_1(t)C_0^*(t)\,M_{10} + h.c.\,, \tag{2-121}$$

where the integrals equal to zero have been canceled and the definition of electric dipole moment that was already used in equation (2-73). Similarly, the density matrix associated with state in equation (2-120) is given by,

$$\rho = |\psi(t)\rangle\langle\psi(t)| =$$

$$\rho = \left(C_1(t)\,|1\rangle + C_0(t)\,|0\rangle\right)\,\left(C_1^*(t)\,\langle 1| + C_0^*(t)\,\langle 0|\right) =$$

$$\rho = |C_1(t)|^2\,|1\rangle\langle 1| + C_1(t)C_0^*(t)\,|1\rangle\langle 0| + C_1^*(t)C_0(t)\,|0\rangle\langle 1| + |C_0(t)|^2\,|0\rangle\langle 0|\,, \tag{2-122}$$

according to equation (2-118), let's calculate the element ρ_{10},

$$\rho_{10} = \langle 1|\rho|0\rangle = C_1^*(t)C_0(t)\,, \tag{2-123}$$

replacing equation (2-123) in (2-121),

$$P_p(t) = M_{01}\,\rho_{10} + h.c. =$$

$$P_p(t) = M_{10}^*\,\rho_{10} + h.c.\,, \tag{2-124}$$

where it has been used that $M_{01} = M_{10}^*$. As in equation (2-119) the rotating wave approximation has been used, in the same way in equation (2-124) we must stay with only one of the terms to be consistent $P_p(t) \approx M_{10}^*\,\rho_{10}$, replacing this result in equation (2-119),

$$\wp_p = 2\,M_{10}^*\,\rho_{10}\,e^{i\omega_p t}\,, \tag{2-125}$$

this result can be equated with the complex polarization definition,

$$\wp_p \equiv \varepsilon_0\,\chi\,\mathcal{E}_p = 2\,M_{10}^*\,\rho_{10}\,e^{i\omega_p t}\,, \tag{2-126}$$

where ε_0 is the vacuum permittivity, χ the system susceptibility and $\mathcal{E}_p$ the field amplitude. Solving for ρ_{10} in (2-126),

$$\rho_{10} = \frac{\varepsilon_0\,\chi\,\mathcal{E}_p}{2\,M_{10}^*}\,e^{-i\omega_p t}\,, \tag{2-127}$$

equating this last equation with (2-118),

$$\frac{iM_{10}\,\mathcal{E}_p\,(\gamma_{02} + i\Delta(\omega_p))\,e^{-i\omega_p t}}{2\hbar[(\gamma_{01} + i\Delta(\omega_p))\,(\gamma_{02} + i\Delta(\omega_p)) + \Omega_c^2/4]} = \frac{\varepsilon_0\,\chi\,\mathcal{E}_p}{2\,M_{10}^*}\,e^{-i\omega_p t}\,,$$

$$\chi = \frac{i|M_{10}|^2\,(\gamma_{02} + i\Delta(\omega_p))}{\hbar\varepsilon_0\,[(\gamma_{01} + i\Delta(\omega_p))\,(\gamma_{02} + i\Delta(\omega_p)) + \Omega_c^2/4]}\,,$$

$$\chi = \frac{i|M_{10}|^2\,\gamma_{02} - |M_{10}|^2\,\Delta(\omega_p)}{\hbar\varepsilon_0\,[\gamma_{01}\,\gamma_{02} + i\gamma_{01}\,\Delta(\omega_p) + i\gamma_{02}\,\Delta(\omega_p) - \Delta(\omega_p)^2 + \Omega_c^2/4]}\,. \tag{2-128}$$

It is necessary to know the real part and the complex part of the susceptibility of the system to calculate the absorption, to obtain these expressions, let's do the substitutions,

$$\alpha = -|M_{10}|^2\,\Delta(\omega_p)\,,$$

$$\beta = |M_{10}|^2\gamma_{02}\,,$$

$$\lambda = \gamma_{01}\gamma_{02} - \Delta(\omega_p)^2 + \Omega_c^2/4\,,$$

$$\sigma = \gamma_{01}\Delta(\omega_p) + \gamma_{02}\Delta(\omega_p)\,,$$

with these substitutions, equation (2-128) takes the simple form,

$$\chi = \frac{\alpha + i\beta}{\hbar\varepsilon_0\,(\lambda + i\sigma)}\,, \tag{2-129}$$

multiplying up and down by $(\lambda - i\sigma)$,

$$\chi = \frac{(\alpha + i\beta)\,(\lambda - i\sigma)}{\hbar\varepsilon_0\,(\lambda + i\sigma)\,(\lambda - i\sigma)}\,,$$

regrouping terms

$$\chi = \frac{(\alpha\lambda + \beta\sigma) - i(\alpha\sigma - \beta\lambda)}{\hbar\varepsilon_0(\lambda^2 + \sigma^2)}\,. \tag{2-130}$$

Defining the susceptibility as $\chi = \chi' + i\,\chi''$, where χ' and χ'' are the real part and imaginary part respectively, with this consideration, of equation (2-130) is obtained that:

$$\chi' = \frac{\alpha\lambda + \beta\sigma}{\hbar\varepsilon_0\left(\lambda^2 + \sigma^2\right)}\,, \tag{2-131}$$

and

$$\chi'' = \frac{\beta\lambda - \alpha\sigma}{\hbar\varepsilon_0\left(\lambda^2 + \sigma^2\right)}\,, \tag{2-132}$$

returning to the original variables,

$$\chi' = \frac{\left(-|M_{10}|^2\,\Delta(\omega_p)\right)\left(\gamma_{01}\gamma_{02} - \Delta(\omega_p)^2 + \Omega_c^2/4\right) + \left(|M_{10}|^2\gamma_{02}\right)\left(\gamma_{01}\Delta(\omega_p) + \gamma_{02}\Delta(\omega_p)\right)}{\hbar\varepsilon_0\left(\left(\gamma_{01}\gamma_{02} - \Delta(\omega_p)^2 + \Omega_c^2/4\right)^2 + \left(\gamma_{01}\Delta(\omega_p) + \gamma_{02}\Delta(\omega_p)\right)^2\right)}\,, \tag{2-133}$$

and

$$\chi'' = \frac{\left(|M_{10}|^2\gamma_{02}\right)\left(\gamma_{01}\gamma_{02} - \Delta(\omega_p)^2 + \Omega_c^2/4\right) - \left(-|M_{10}|^2\,\Delta(\omega_p)\right)\left(\gamma_{01}\Delta(\omega_p) + \gamma_{02}\Delta(\omega_p)\right)}{\hbar\varepsilon_0\left(\left(\gamma_{01}\gamma_{02} - \Delta(\omega_p)^2 + \Omega_c^2/4\right)^2 + \left(\gamma_{01}\Delta(\omega_p) + \gamma_{02}\Delta(\omega_p)\right)^2\right)}\,, \tag{2-134}$$

simplifying, the real part of the susceptibility is finally obtained as,

$$\chi'(\omega_p) = \frac{\Xi\,\Delta(\omega_p)}{\Theta(\omega_p)}\,\left[\Delta(\omega_p)^2 + \gamma_{02}^2 - \Omega_c^2/4\right]\,, \tag{2-135}$$

similarly, the imaginary part of susceptibility,

$$\chi''(\omega_p) = \frac{\Xi}{\Theta(\omega_p)}\,\left[\gamma_{02}\,\left(\Omega_c^2/4 + \gamma_{01}\gamma_{02}\right) + \Delta(\omega_p)^2\gamma_{01}\right]\,, \tag{2-136}$$

where $\Xi = \sigma_{01}|\mathrm{M}_{01}|^2/\epsilon_0\hbar$,
$\Theta(\omega_p) = \left[(|\Omega_c|^2/4) + \gamma_{01}\gamma_{02} - \Delta(\omega_p)^2\right]^2 + \Delta(\omega_p)^2(\gamma_{01} + \gamma_{02})^2$, γ_{ij} are the decay rates and are related to the natural decay rates of the i, j states, and $\Delta(\omega_p) =$

$[(E_1-E_0)-\hbar\omega_p]/\hbar$ is the detuning of the system with the probe field. Note that in Ξ, σ_{01} has been added which corresponds to the three-dimensional electronic concentration.
When $\Delta(\omega_p)=0$, which indicates that the probe field is in resonance with the transition between states $|0\rangle$ and $|1\rangle$, it is obtained,

$$\chi' = 0 \quad \text{and} \quad \chi'' = \frac{\Xi\,\gamma_{02}}{\gamma_{01}\gamma_{02}+\Omega_c^2/4}\,. \tag{2-137}$$

It is evident that the imaginary part of the susceptibility is proportional to γ_{02}, remembering that γ_{02} is the decay rate between states $|0\rangle$ and $|2\rangle$ and since these states are not coupled, then $\gamma_{02}\to 0$ which implies that $\chi''\approx 0$. The above indicates that the absorption tends to zero, thus the radiation is not being absorbed when the system is in resonance with the probe field ($\omega_{10}=\omega_p$), the system behaves as if it were transparent to this radiation (remembering that this should be the point of maximum absorption). This process is known as electromagnetically induced transparency. The effect depends on the Rabi frequency of the drive field and the decay rate between states $|0\rangle$ and $|2\rangle$.
By using the intensity of the electromagnetic field associated with a wave of amplitude E_c (control field) $I_c = c\,\epsilon_0|E_c|^2/2$, an expression is obtained for the intensity of the electromagnetic wave as a function of the associated Rabi frequency and the dipole element $|\mathrm{M}_{12}|$ that couples the states Ψ_1 and Ψ_2,

$$I_c = \frac{c\,\epsilon_0\,\hbar^2}{2}\,\frac{|\Omega_c|^2}{|\mathrm{M}_{12}|^2}\,, \tag{2-138}$$

in this work the value of the Rabi frequency Ω_c has been fixed [24], which implies that the intensity of the electromagnetic radiation (control field) is inversely proportional to the square of the dipole element. An equivalent expression to (2-138) is obtained for the probe field intensity by using $|\Omega_p|$ and $|\mathrm{M}_{01}|$. From equation (2-136) an expression for the system absorption is obtained,

$$\alpha_{EIT}(\omega_p) = (\omega_p/c)\,\chi''(\omega_p)\,, \tag{2-139}$$

where c is the speed of light in a vacuum. All the parameters associated with the EIT calculation are included in Table **3-1** in the 3.1 section [25, 26].

It is worth mentioning some of the potential applications of the EIT in both theoretical and experimental developments. In 2004 at Hewlett-Packard Laboratories, Beausoleil *et al.* [27] developed a general outline of the requirements that components produced for industrial-level quantum information technology (QIT) must have, the authors identified EIT as a possibility that facilitates the goal of providing quantum information processing of few qubits. Later in 2011, Safavi-Naeini *et al.* [28] by means of interaction control techniques between localized optics and mechanical excitations have obtained experimental advances in micro and nanofabrication techniques. These authors demonstrate the presence of EIT and tunable optical delays (slow and stopped light) in an optomechanical crystal of the order of nanometers, using optomechanical nonlinearity to control the speed of light through an experimental design to modulate photon-phonon interaction. Another significant application of the EIT is in sensors [29], in recent years Yan *et al.* [30] proposed a kind of biosensor based on EIT as metamaterial, this device emerged good efficiency for detection of some cancer cells.

2.4. Finite difference method (FDM)

The FDM is widely used for solving differential equations. The advantage of implementing this method is to convert the differential equation into a set of algebraic equations that can be solved by any matrix or diagonalization method. Figure **2-5** represents a scheme in which the function $f(x)$ (red curve) has been discretized in a set of points according to an equidistant grid $N+1$ points on the x-axis, in such form that is fulfilled by definition: $f_j \equiv f(x_j)$ for all x_j in the interval (x_0, x_N).

From the above, it clearly follows that each point x_j can be represented as $x_j = x_0 + j\Delta x$. The starting point for the development of the method consists of the ordinary definition of the first-order derivative at a x_k point using central differences: $df(x_k)/dx = \lim_{\Delta x \to 0}[f(x_k + \Delta x) - f(x_k - \Delta x)]/2\Delta x$. In the limit in which $\Delta x \acute{}1$, we can to approximate the derivative at a x_k point as:

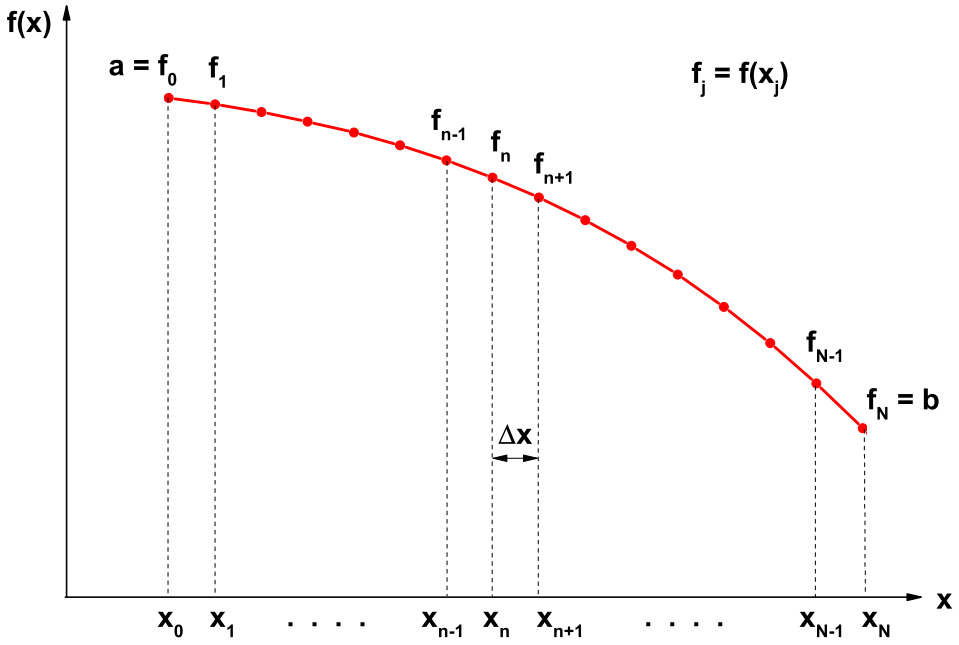

Figure 2-5.: Representative schematic of a one-dimensional point mesh used to develop the finite difference method.

$$\frac{df(x_k)}{dx} \approx \frac{f(x_{k+1}) - f(x_{k-1})}{2\Delta x} = \frac{f_{k+1} - f_{k-1}}{2\Delta x}\,. \tag{2-140}$$

To ensure good precision in the results, it is necessary that the parameter Δx be much smaller than the size of the interval corresponding to the domain of x, that is, it must be true that $\Delta x \ll (x_N - x_0)$. According to equation (2-140), this is a well-known expression to represent the first derivative of a function at the point x_k. Analogously, we can start from the derivative expression using forward differences or backward differences to obtain the second derivative of a function $f(x)$ at a point x_k through central differences, i.e.,

$$\frac{d^2 f(x_k)}{dx^2} \approx \frac{\frac{f_{k+1} - f_k}{\Delta x} - \frac{f_k - f_{k-1}}{\Delta x}}{\Delta x} = \frac{f_{k-1} - 2f_k + f_{k+1}}{\Delta x^2}\,. \tag{2-141}$$

In this way, an expression is found to calculate the second derivative of a function $f(x)$ at the point x_k by means of central differences. Note that in equations

(2-140) and (2-141), k can take integer values only in the interval $(1, N-1)$. The terms f_0 and f_N correspond to boundary conditions (see the Figure **2-5**) for the function with values a and b that are assumed to be known: $f_0 = f(x_0) = a$ and $f_N = f(x_N) = b$. Evaluating equations (2-140) and (2-141) for some k values, it is easy to show that the first and second derivatives of a function on the given interval can be written in matrix form

$$\frac{df(x)}{dx} = \frac{1}{2\Delta x}\begin{pmatrix} 1 & 0 & 0 & 0 & 0 & 0 & \cdots & 0 & 0 \\ -1 & 0 & 1 & 0 & 0 & 0 & \cdots & 0 & 0 \\ 0 & -1 & 0 & 1 & 0 & 0 & \cdots & 0 & 0 \\ 0 & 0 & -1 & 0 & 1 & 0 & \cdots & 0 & 0 \\ \vdots & & \vdots & & \ddots & & \vdots & & \vdots \\ 0 & 0 & 0 & 0 & 0 & \cdots & 0 & -1 & 1 \\ 0 & 0 & 0 & 0 & 0 & 0 & \cdots & 0 & 1 \end{pmatrix}\begin{pmatrix} f_0 \\ f_1 \\ f_2 \\ f_3 \\ \vdots \\ f_{N-1} \\ f_N \end{pmatrix} \tag{2-142}$$

and

$$\frac{d^2f(x)}{dx^2} = \frac{1}{\Delta x^2}\begin{pmatrix} 1 & 0 & 0 & 0 & 0 & 0 & \cdots & 0 & 0 & 0 \\ 1 & -2 & 1 & 0 & 0 & 0 & \cdots & 0 & 0 & 0 \\ 0 & 1 & -2 & 1 & 0 & 0 & \cdots & 0 & 0 & 0 \\ 0 & 0 & 1 & -2 & 1 & 0 & \cdots & 0 & 0 & 0 \\ \vdots & & \vdots & & \ddots & & \vdots & & \vdots & \\ 0 & 0 & 0 & 0 & 0 & \cdots & 0 & 1 & -2 & 1 \\ 0 & 0 & 0 & 0 & 0 & 0 & \cdots & 0 & 0 & 1 \end{pmatrix}\begin{pmatrix} f_0 \\ f_1 \\ f_2 \\ f_3 \\ \vdots \\ f_{N-1} \\ f_N \end{pmatrix}. \tag{2-143}$$

Relations (2-142) and (2-143) are the matrix representation of the first and second derivatives, respectively, of a function $f(x)$ on the interval (x_0, x_N) with boundary conditions $f(x_0) = a$ and $f(x_N) = b$. By means of this last representation of the second derivative, we need to solve the equations (2-57) and (2-60) at each self-consistent step.

According to the relation (2-141), Schrödinger's formulation (2-57) can be rew-

ritten in finite differences as:

$$-\frac{\hbar^2}{2\,m^*}\left(\frac{\psi_{k-1}-2\psi_k+\psi_{k+1}}{\Delta x^2}\right)+\mathcal{V}_k\psi_k=E\psi_k\,, \tag{2-144}$$

considering $x \in [a,b]$, this equation must satisfy the boundary conditions $\psi_0=\psi_N=0$ to cancel the wave function at $\pm\infty$.
Below are the corresponding definitions to consistency, stability, and convergence for a finite difference scheme [31, 32]:
Schema consistency The numerical scheme consistency means that the solution using the finite difference scheme approaches the exact equation solution, that is, the discretization error tends to zero when the interval of the mesh continuously decreases.
Schema stability The stability determines the increase or decrease of the numerical errors that are committed when solving the equation in finite differences. Although an equation in theoretically has an exact solution, rounding errors are made in numerical resolution. If the errors smooth out as the calculations are performed, the scheme is stable; however, if they do not remain bounded, the scheme is unstable.
Schema convergence The numerical solution converges to the analytical solution when the former tends to the latter when the mesh is refined.
Lax-Richtmyer Equivalence Theorem A consistent finite difference scheme for a partial differential equation such that the initial value problem is well stated is convergent if and only if it is stable [33].
In the solution of this work, the eigenvalues and wave functions have been calculated using the Schrödinger equation in finite differences (equation 2-144), the stability of this equation in finite differences has been corroborated in various works, normally using the Von Neumann stability criterion [34], for which, according to the Lax-Richtmyer theorem, the solution convergence to the numerical problem is guaranteed.

References

[1] Römer, M.; Bernien, H.; Müller, G.; Schuh, D.; Hübner, J.; Oestreich, M. Electron-spin relaxation in bulk GaAs for doping densities close to the metal-to-insulator transition, *Phys.Rev. B* **2010**, *81*, 075216.

[2] Dakhlaoui, H.; Belhadj, W.; Durmuslar, A. S.; Ungan, F.; Abdelkader, A. Numerical study of optical absorption coefficients in Manning-like AlGaAs/GaAs double quantum wells: Effects of doped impurities, *Physica E Low Dimens. Syst. Nanostruct.* **2023**, *147*, 115623.

[3] Dakhlaoui, H. , The effects of doping layer location on the electronic and optical properties of GaN step quantum well, *Superlattices Microstruct.* **2016**, *97*, 439-447.

[4] Mitin, V. V.; Kochelap, V. A.; Stroncio, M. A. Introduction to Nanoelectronics, Science, Nanotechnology, Engineering, and Applications, *Cambridge University Press* **2008**, ISBN-10 0-511-36811-9, p. 205.

[5] Ahn, D.; Chuang, S. L. Intersubband optical absorption in a quantum well with an applied electric field, *Phys. Rev. B* **1987**, *35*, 4149-4151.

[6] Dakhlaoui, H.; Gil-Corrales, J. A.; Morales, A. L.; Kasapoglu, E.; Radu, A.; Restrepo, R. L.; Tulupenko, V.; Vinasco, J. A.; Mora-Ramos, M. E.; Duque, C. A. Theoretical study of electronic and optical properties in doped quantum structures with Razavy confining potential: effects of external fields, *J. Comput. Electron.* **2022**, *21*, 378–395.

[7] Dakhlaoui, H.; Belhadj, W.; Durmuslar, A. S.; Ungan, F.; Abdelkader, A. Numerical study of optical absorption coefficients in Manning-like AlGaAs/GaAs double quantum wells: Effects of doped impurities, *Physica E Low Dimens. Syst. Nanostruct.* **2023**, *147*, 115623.

[8] Shao, Y.; Solin, S. A.; Ram-Mohan, L. R. Carrier Mobilities in Delta-doped Heterostructures, *cond-mat.mtrl-sci* **2006**, pp. 8.

[9] D. Ahn and S.-L. Chuang, Calculation of linear and nonlinear intersubband optical absorptions in a quantum well model with an applied electric field, *IEEE J. Quantum Elect.* **1987**, **23**, 2196.

[10] Stern, F. Elementary theory of the optical properties of solids, *Solid State Phys.* **1963**, **15**, 299-408.

[11] Kan, Y.; Nagal, H.; Yamanishi, M.; Suemune, I. Field effects on the refractive index and absorption coefficient in AlGaAs quantum well structures and their feasibility for electrooptic device applications, *IEEE J. Quantum Elect.* **1987**, **12**, 2167-2180.

[12] R. Loudon, The Quantum Theory of Light *Oxford University Press* **2000**, ISBN 0 19 850177 3.

[13] R. Loudon, Intersubband resonant enhancement of the nonlinear optical properties in asymmetric (CdS/ZnSe)/X-BeTe based quantum wells, *Opt. Mater.* **2013**, **35**, 875-880.

[14] Ponomarev, I. V.; Deych, L. I.; Shuvayev, V. A.; Lisyansky, A. A. Self-consistent approach for calculations of exciton binding energy in quantum wells. *Physica E* **2005**, *25*, 539–55.

[15] Shuvayev, V. A.; Deych, L. I.; Ponomarev, I. V.; Lisyansky, A. A. Self-consistent Hartree method for calculations of exciton binding energy in quantum wells, *Superlattices Microstruct.* **2006**, *40*, 77–92.

[16] Dujardin, F.; Assaid, E.; Feddi, E. New way for determining electron energy levels in quantum dots arrays using finite difference method, *Superlattices Microstruct.* **2018**, *118*, 256-265.

[17] Ahn, J. S. Finite difference method for the arbitrary potential in two dimensions: Application to double/triple quantum dots, *Superlattices Microstruct.* **2014**, *65*, 113–123.

[18] Mukherjee, R.; Konar, S. Electromagnetically induced transparency based quantum well infrared photodetectors, *J. Lumin.* **2022**, *251*, 119176.

[19] Bashir, A. I. Role of intense laser-excited dressed states via electromagnetically induced transparency on the Fresnel-Fizeau photon drag through an asymmetric double quantum dot molecule (GaAs/AlGaAs) in the Λ-type configuration, *Physica E* **2021**, *134*, 114904.

[20] Harris, S. E.; Field, J. E.; Imamoglu, A. Nonlinear optical processes using electromagnetically induced transparency, *Phys. Rev. Lett.* **1990**, *64*, 1107-1110.

[21] Armstrong, J. A.; Wynne, J. J. Autoionizing states of Sr studied by the generation of tunable vaccum uv radiation, *Phys. Rev. Lett.* **1974**, *33*, 1183-1185.

[22] Scully, M.; Zubairy, M. Quantum Optics, *Cambridge University Press* **1997**, ISBN-13: 978-0524235959.

[23] Gambhir, M.; Gumber, S.; Jha, P. K.; Mohan, M. Dependence of electromagnetically induced transparency on pressure and temperature in a quantum dot with flat cylindrical geometry, *Superlattices Microstruct.* **2014**, *71*, 147–161.

[24] Al, E. B.; Kasapoglu, E.; Sari, H.; Sökmen, I.; Duque, C. A.; Binding Energy and Absorption of Donor Impurity in Spherical GaAs/$Al_xGa_{1-x}As$ Quantum Dots With Konwent Potential, *Research square* **2021**.

[25] Al, E. B.; Kasapoglu, E.; Sari, H.; Sökmen, I. Optical properties of spherical quantum dot in the presence of donor impurity under the magnetic field, *Physica B* **2021**, *613*, 412874.

[26] Bejan, D. Effects of electric field and structure on the electromagnetically induced transparency in double quantum dot, *Opt. Mater.* **2017**, *67*, 145-154.

[27] Beausoleil, R. G.; Munro, W. J.; Rodrigues, D. A.; Spiller, T. P. Applications of electromagnetically induced transparency to quantum information processing, *J. Mod. Opt.* **2004**, *51*, 16-18.

[28] Safavi-Naeini, A. H.; Mayer Alegre, T. P.; Chan, J.; Eichenfield, M.; Winger, M.; Lin, Q.; Hill, J. T.; Chang, D. E.; Painte, O. Electromagnetically induced transparency and slow light with optomechanics, *Nature.* **2011**, *472*, 69-73.

[29] Wu, D.; Liu, Y.; Yu, L.; Yu, Z.; Chen, L.; Li, R.; Ma, R.; Liu, C.; Zhang, J.; Ye, H. Plasmonic metamaterial for electromagnetically induced transparency analogue and ultra-high figure of merit sensor, *Sci. Rep.* **2017**, *7*, 45210.

[30] Yan, X.; Yang, M.; Zhang, Z.; Liang, L.; Wei, D.; Wang, M.; Zhang, M.; Wang, T.; Liu, L.; Xie, J.; et al. The terahertz electromagnetically induced transparency-like metamaterials for sensitive biosensors in the detection of cancer cells, *Biosens. Bioelectron.* **2019**, *126*, 485-492.

[31] Sora, F.; Uriza, M. Estudio numérico del modelo de Heston: método de diferencias finitas, *Universidad EAFIT* **2013**, tesis de maestría.

[32] Lara, L.; Chávez, Z.; Castañeda, J. El método de diferencias finitas. Teoria y Práctica, *UPAO* **2019**, 2019-17206.

[33] Lax, P. D.; Richtmyer, R. D.; Survey of the stability of linear finite difference equations. *Comm. Pure Appl. Math.* **1956**, *IX*, 267-293.

[34] Zhao, H.; Gao, J.; Chen, Z. Stability and numerical dispersion analysis of finite-difference method for the diffusive-viscous wave equation. *Int. J. Numer. Anal. Model.* **2014**, *5*, 66-78.

3. Results and discussion

3.1. Energies and probability density by changing L, n_d, δ and ξ

Table **3-1** details the parameters used throughout the work, γ_{01} and γ_{02} parameters corresponding to the decay rates, and have been taken according to the GaAs and AlGaAs materials referencing to the work of E. B. Al *et al.* [1] and D. Bejan *et al.* [2], likewise, the τ_{in} relaxation time has been referenced from the reports of E.B. Al *et al.* [3] and H. Dakhlaoui *et al.* [4], approximating a constant value since the range of variation of donor density is relatively small. The doping levels that have been used for the calculation are in a high doping regime, but their order of magnitude is not a novelty for investigations in this type of heterostructures, both experimentally and theoretically, as evidenced by Y. A. Aleshchenko *et al.* [5], H. Dakhlaoui [6], and R. B. Dhafera *et al.* [7].

It should be noted that in this work, the same effective mass has been assumed for both the well and barrier regions, as well as the dielectric constant. These approximations do not modify the physics of the results, which is one of the main objectives of analyzing in this work. Also, for the GaAs/AlGaAs heterostructure with 30 % Al, the difference in effective masses and dielectric constants does not definitively modify the system's energies.

Parameter	Value
$\hbar$	1.054×10^{-34} (J s)
m^*	$0.067\, m_0$ (Kg)
m_0	9.109×10^{-31} (Kg)
e	1.602×10^{-19} (C)
k_B	1.381×10^{-23} (J/K)
ϵ_0	8.854×10^{-12} (F/m)
ϵ	12.35
V_0	0.228 (eV)
T	300 (K)
c	299'792.458 (m/s)
γ_{01}	0.1 (THz)
γ_{02}	5 (THz)
Ω_c	40 (THz)
τ_{in}	0.14 (ps)
μ	$4\pi\times10^{-7}$ (H/m)

Table 3-1.: List of parameters used in the calculations.

In Figure **3-1** are depicted the lowest energy levels for a confined electron in a GaAs/AlGaAs as a function of the well-width considering a delta layer at the well center, Figure **3-1(b)**. Figures **3-1(a)** and **3-1(c)** show the confinement potential and the probability density for $L = 10\,\text{nm}$ and $L = 25\,\text{nm}$, respectively. Figure **3-1(a)** shows the conduction band bottom profile without including the donor layer (dashed black curve) for $L = 10\,\text{nm}$, on-center donor layer with $\delta = 2\,\text{nm}$, and donor density $\text{n}_d = 4.5 \times 10^{25}\,(1/\text{m}^3)$. This profile structure is modified (continuous navy color curve), causing a sharp profile in the center of the well and a systematic decrease in the barrier regions. The shaded region corresponds to the system-occupied states. The self-consistent Fermi level takes an approximate value of 0.175 eV. Additionally, the probability densities associated with the first three confined states have been presented (black, red, and green curves). Note that only the Ψ_0 and Ψ_1 states are occupied. It is evident that by including the effect of the doped delta layer, a redshift is induced in all states due to the decrease in the value of the conduction band bottom. Figure

3-1(c) is equivalent to Figure **3-1(a)**, but for $L = 25\,\text{nm}$. Note that with this increase in the well width, the number of confined states increases, which is to be expected since the confinement is decreased. On the other hand, there is a decrease in the Fermi level, being now approximately $0.065\,\text{eV}$ and presenting an occupation of three states instead of two as occurs for the case $L = 10\,\text{nm}$. For the greater value of the well width, there are no significant modifications in the barrier region (AlGaAs); this is due to the location of the delta layer in the central region of the well and the condition of zero electrostatic potential at infinities, that is, the band offset potential is much greater than the electrostatic potential in these regions. A different situation occurs in the quantum well region, in which the electrostatic potential significantly modifies the bottom of the well, accommodating the lowest states in this region (see the black and red curve in Figure **3-1(c)**). Note how the electronic probability is concentrated almost entirely inside the well generated by the delta layer. Figure **3-1(b)** shows the energy spectrum as a function of the well width, keeping the other parameters fixed: $\xi = 0$, $\delta = 2\,\text{nm}$, and $n_d = 4.5\times10^{25}\,(1/\text{m}^3)$. A monotonic decrease is evident for all confined states (states inside the well). This is due to a decrease in confinement caused by the increase in the well width. The dashed black line represents the Fermi-level behavior with the increase of L. It is observed that the system with $L = 10\,\text{nm}$ presents only two occupied states, as previously mentioned. For a well width greater than $13\,\text{nm}$, the system already presents three occupied states. Note how the difference in energy between the states becomes smaller with the increase in L. This behavior is due to the fact that the decrease in confinement allows the entry of new eigenvalues from the continuum towards the interior of the quantum well, causing the energies to become closer.

In Figure **3-2** are depicted the lowest energy levels for a confined electron in a GaAs/AlGaAs as a function of the on-center δ-parameter, Figure **3-2(b)**. Figures **3-1(a)** and **3-1(c)** show the confinement potential and the probability density for $\delta = 1\,\text{nm}$ and $\delta = 5\,\text{nm}$, respectively. Figure **3-2(a)** shows the profile of the conduction band bottom for a quantum well of width $L = 10\,\text{nm}$, not including the doped delta layer (black dashed curve). This profile corresponds to the electron confinement potential $\mathcal{V}_c(x)$ before starting the self-consistent process required to solve the system, including a donor density. The potential

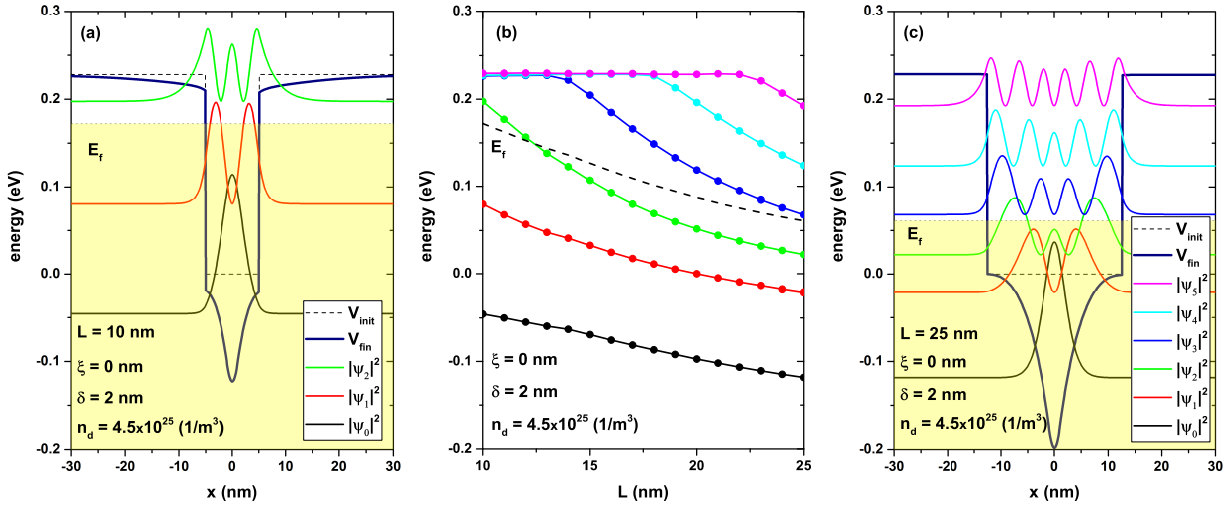

Figure 3-1.: **(a)** and **(c)**: Self-consistent potential $\mathcal{V}(x)$ with a solid line in navy color, and electron confinement potential $\mathcal{V}_c(x)$ in black dashed line. Figure **(a)** corresponds to $L = 10\,\text{nm}$ and figure **(c)** to $L = 25\,\text{nm}$; for both figures the parameters $\xi = 0$, $n_d = 4.5\times10^{25}\,(1/\text{m}^3)$, and $\delta = 2\,\text{nm}$ have been set. In both figures, the probability densities of all confined states have been included. The shaded region indicates the occupied states and the maximum of said region corresponds to the energy Fermi level in the system. Figure **(b)** represents the lowest confined energy levels as a function of the well width; the dashed line is the self-consistent Fermi level E_f.

profile after self-consistency of the same quantum well, including a doped delta layer in the center ($\xi = 0$) is shown in navy color, width $\delta = 1\,\text{nm}$ and $n_d = 4.5 \times 10^{25}\ (1/\text{m}^3)$. The shaded region represents the occupied states and the curves in black, red, and green colors represent the probability density associated with the lowest three confined states, respectively. Figure **3-2(c)** shows the same system but with $\delta = 5\,\text{nm}$, that is, the region in which the donor density is distributed has been increased. Clearly, for a region of 5 nm it no longer makes sense to talk about a delta type doping; this is a whole doped region. The most evident effect is observed in the depth of the quantum well, which now presents the bottom at approximately -0.24 eV, as the energy zero remains fixed at the bottom of the electron confinement potential; there is a clear decrease in the system energy comparing with the system of $\delta = 1\,\text{nm}$. This modification in the bottom of the conduction band induces the appearance of new confined states, as shown in Figure **3-2(c)**, the Ψ_3 state (blue color curve). On the other hand, since the volume of the doped layer has been increased, keeping the donor density fixed, this implies that the number of charge carriers must increase and therefore the Fermi level in the system must also increase, this is evidenced in the shaded region that now takes a much higher value even above the bottom of the band in the barrier region, causing a full occupation of all confined states. Figure **3-2(b)** shows the energy spectrum corresponding to the confined states in the quantum well as a function of the width of the δ-parameter, holding fixed $L = 10\,\text{nm}$, $\xi = 0$, and $n_d = 4.5 \times 10^{25}\,(1/\text{m}^3)$. The dashed line corresponds to the system Fermi level that presents a monotonically increasing behavior, as already mentioned. All the states present a red shift in energy, the shift being more abrupt for lower states; for example, the ground state presents a shift of approximately 0.16 eV. This decrease in energies, despite having a clear increase in confinement with the increase in the δ-parameter, is because the energy is measured concerning the bottom of the electron confinement potential $\mathcal{V}_c(x)$ (dashed line in Figure **3-2(a)**) and not for the lowest point of the conduction band that would correspond to the center of the doped layer.

In Figure **3-3** are depicted the lowest energy levels for a confined electron in a GaAs/AlGaAs as a function of the on-center ξ-parameter, Figure **3-3(b)**. Figures **3-3(a)** and **3-3(c)** show the confinement potential and the probability

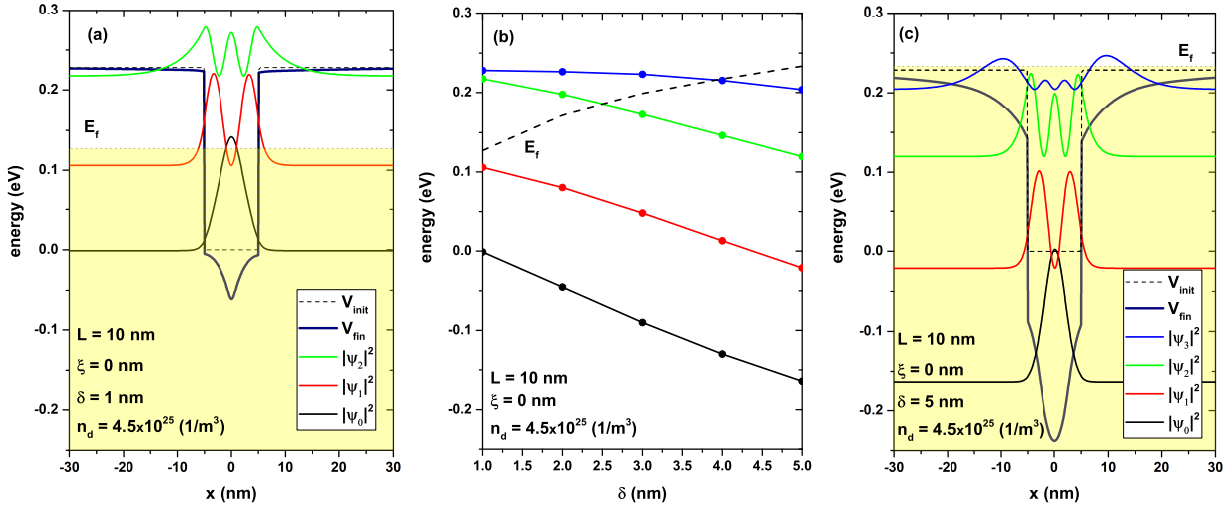

Figure 3-2.: **(a)** and **(c)**: Self-consistent potentials $\mathcal{V}(x)$, with a solid line in navy color, and electron confinement potential $\mathcal{V}_c(x)$ in black dashed line. Figure **(a)** corresponds to $\delta = 1\,\text{nm}$ and Figure **(c)** to $\delta = 5\,\text{nm}$. For both figures the parameters $L = 10\,\text{nm}$, $\xi = 0$, and $n_d = 4.5\times\ 10^{25}\,(1/\text{m}^3)$ have been set. In both figures, the probability densities of all confined states have been included. The shaded region indicates the occupied states, and the maximum of said region corresponds to the energy Fermi level. Figure **(b)** represents the energy of the confined states concerning the δ-parameter; the dashed line is the self-consistent Fermi level E_f.

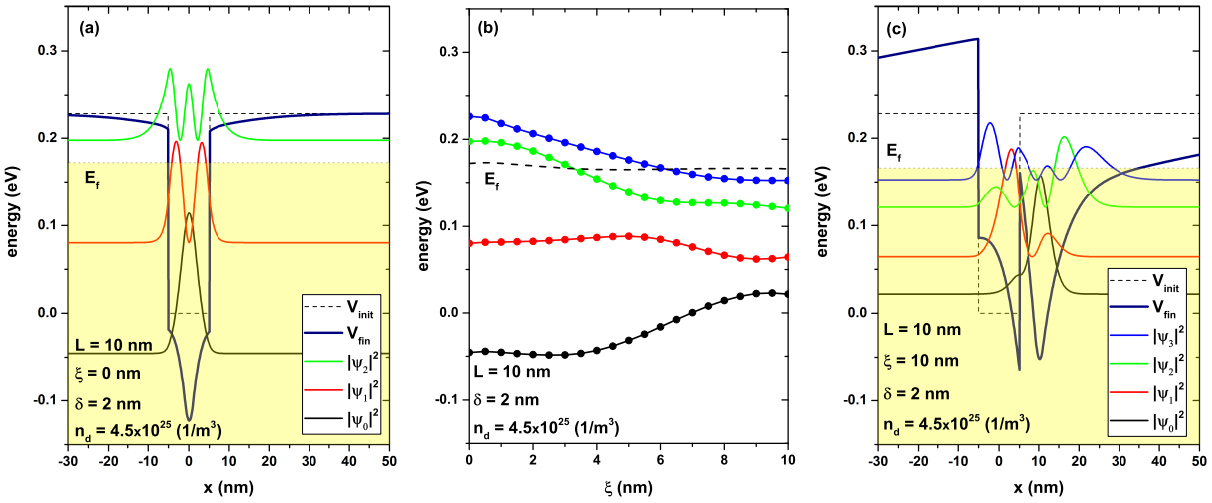

Figure 3-3.: **(a)** and **(c)**: Self-consistent potentials $\mathcal{V}(x)$ with a solid line in navy color, and electron confinement potential $\mathcal{V}_c(x)$ in black dashed line. Figure **(a)** corresponds to $\xi = 0$ and Figure **(c)** to $\xi = 10\,\text{nm}$. For both figures the parameters $L = 10\,\text{nm}$, $n_d = 4.5\times\ 10^{25}\,(1/\text{m}^3)$, and $\delta = 2\,\text{nm}$ have been set. In both figures, the probability densities of some confined states have been included. The shaded region indicates the occupied states and the maximum of said region corresponds to the energy Fermi level. Figure **(b)** represents the lowest confined energy levels as a function of the ξ-parameter; the dashed line is the self-consistent Fermi level E_f.

density for $\xi = 0$ and $\xi = 10\,\text{nm}$, respectively. Figure **3-3(a)** is the same Figure **3-1(a)** with a different scale that has been placed for comparison purposes with figure **3-3(c)**. This shows the quantum well with delta doping keeping fixed $L = 10\,\text{nm}$, $\xi = 0$, and $n_d = 4.5{\times}10^{25}\,(1/\text{m}^3)$. Figure **3-3(c)** shows the same system but now locating the doped delta layer at $\xi = 10\,\text{nm}$, that is, it is 5 nm outside the edge of the well. The fact of moving the delta layer to the right causes the loss of symmetry in the system; a direct implication of this is that the wave functions also lose symmetry. In this case, an accumulation of charge carriers is generated in the region where the delta layer is located, causing an electrostatic potential with a significantly high value at that point (comparable with the confinement potential V_0) and as a consequence of this, the total self-consistent potential (sum of confinement potential and Hartee potential) is generated for a double-well system as seen in Figure **3-3(c)**. In the AlGaAs barrier region occurs a clear asymmetry in the potential, being $\mathcal{V}(x) > V_0$ for $x < -5\,\text{nm}$ and $\mathcal{V}(x) < V_0$ for $x > 10\,\text{nm}$; this difference in electronic confinement causes the probability density associated with the ground state to accumulate to a greater extent in the well-produced by the delta layer (the electrons tend to be located in the place of least confinement), around $x = 10\,\text{nm}$. Note how the opposite occurs with the first excited state, which remains with high density inside the GaAs well in -5 nm$< x <$5 nm.

On the other hand, the Fermi level practically does not change with the displacement of the delta layer; this is because the change in ξ does not modify the number of charge carriers. However, this fact does not imply that the number of occupied states can be modified, as can be seen in Figure **3-3(a)**, there are two occupied states while in Figure **3-3(c)**, there are already four occupied states. The fact of locating the delta layer in a position that breaks the symmetry of the system generates a break in the symmetry of the self-consistent potential ($\mathcal{V}(x)$); this is mainly caused by the electrostatic potential that now presents a high asymmetry, drastically modifying the electron confinement potential of the well. In Figure **3-3(b)**, we see the energies of the first four confined states as a function of the position of the ξ-parameter, keeping the other parameters fixed at $L = 10\,\text{nm}$, $\delta = 2\,\text{nm}$, and $n_d = 4.5{\times}10^{25}\,(1/\text{m}^3)$. The Fermi level corresponds to the dashed line, and this remains practically fixed, as already stated, since there is no change in the number of carriers or in the temperature

of the system. Note how the ground state and the first excited state (black and red curves, respectively) remain approximately unchanged in the range $0 \leq \xi < 5\,\text{nm}$; this is the range in which the delta layer is moved from the center to the edge of the quantum well and there is no change in the depth of the well. Already for the range $\xi > 5\,\text{nm}$, these two states tend to come together; this is because the delta layer comes out of the well, giving rise to the origin of a new quantum well, and the system behaves as a coupled double quantum well system.

In Figure **3-4** are shown the lowest energy levels for a confined electron in a GaAs/AlGaAs as a function of the on-center n_d-parameter, Figure **3-4(b)**. Figures **3-4(a)** and **3-4(c)** show the confinement potential and the probability density for $n_d = 1.0\times\ 10^{25}\,(1/\text{m}^3)$ and $n_d = 4.5\times\ 10^{25}\,(1/\text{m}^3)$, respectively. Figure **3-4(a)** shows the quantum well system with $L = 10\,\text{nm}$, $\xi = 0$, $\delta = 2\,\text{nm}$, and $n_d = 1.0\times 10^{25}\,(1/\text{m}^3)$. As the donor density is lower, there is no significant change in the barrier regions and in the well, only a decrease of approximately 0.06 eV. The Fermi level must change when the donor density decreases; in this case, it takes a value of 0.13 eV (shaded region) and corresponds to the occupation of the ground state (see the black curve in Figure **3-4(a)**). Figure **3-4(c)** shows the same system but now increasing the donor density to $n_d = 4.5\times 10^{25}\,(1/\text{m}^3)$, keeping the other parameters the same. Firstly, it is evident that the increase in donor density generates a deeper quantum well inside the initial well (compare $\mathcal{V}_c(x)$ with $\mathcal{V}(x)$). On the other hand, the states present a slight decrease concerning zero energy, and the probability density tends to be a little more localized around the point $x = 0$. In Figure **3-4(b)**, the energy levels are presented as a function of the donor density n_d for the first three states, fixing the width of the well, the position of the delta layer, and the width of the delta layer. The Fermi level again corresponds to the dashed line and presents a monotonically increasing behavior which is the result of the increase in the number of charge carriers with the increase of n_d. For the lowest density, i.e., for $n_d = 1.0\times 10^{25}\,(1/\text{m}^3)$, only the ground state is occupied; for $n_d > 1.75 \times 10^{25}\,(1/\text{m}^3)$ there begins to be an occupation of the first excited state. As the donor density increases, the bottom of the well begins to decrease towards lower energies, like all confined states. However, it should be noted that

the relative distance between the bottom of the conduction band (bottom of the quantum well) and each one of the states presents an increase originated by the increase in confinement; that is, the electrons feel a greater height well with the increase of n_d.

Note how the redshift in the ground state is a little more pronounced than that corresponding to the first excited state with the increase in donor density, this implies that the intersubband spacing E_{21} increases and therefore, it is expected that a blue shift is generated in the optical absorption peaks (Figure **3-7**(**d**)), similarly the increase in the electron density in the ground state causes an increase in the intensity of the absorption peaks, as will be seen later. It should be noted that this behavior has been experimentally demonstrated [8] and in uniformly doped QWs, the enhancement of intersubband transition energy with N_d is mainly attributed to a depolarization shift effect, which is a many-particle effect [9, 10].

3.2. Hartree potential and electron density

Figure **3-5** shows the self-consistent Hartree potential as a function of position x. In **(a)** varying the L, in **(b)** varying the δ, in **(c)** varying the ξ, and in **(d)** varying the n_d. In each case, when one parameter is changed, the others are set to $L = 10\,\text{nm}$, $\xi = 0$, $\delta = 2\,\text{nm}$, and $n_d = 4.5{\times}10^{25}\,(1/\text{m}^3)$. All figures **3-5**(**a**-**d**) have been put on the same scale for comparison purposes. Note that the Hartree potential with the smallest value is the one corresponding to $n_d = 1.0{\times}10^{25}\,(1/\text{m}^3)$ (black curve in Figure **3-5**(**d**)), that is, with this density value of the delta layer, there are no major modifications in terms of the bottom profile of the conduction band, since it is a value comparable to the electron confinement potential (V_0); this has been shown previously in Figure **3-4**(**a**) comparing the potentials $\mathcal{V}_c(x)$ and $\mathcal{V}(x)$. The increase in the donors density generates an increase in the electrostatic potential, as can be seen in the red curve of Figure **3-5**(**d**). This is due to the increase in the charge density associated with the increase in the donor density and the electronic occupation of the ground state and the first excited state generated by the increase in Fermi energy, this is evidenced in figures **3-4**(**a**) and **3-4**(**c**). Figure **3-5**(**b**) shows the

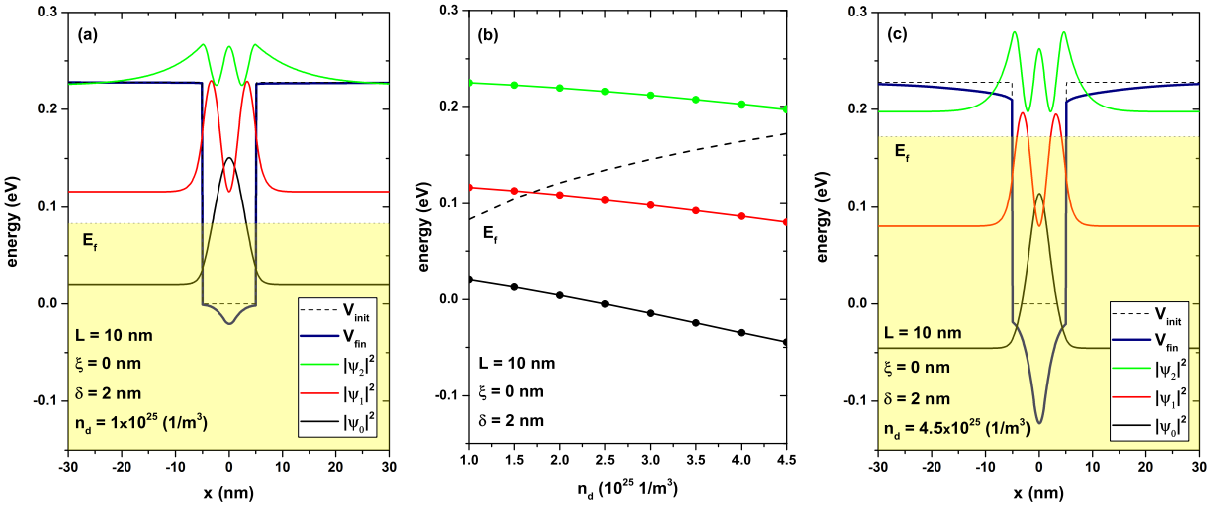

Figure 3-4.: **(a)** and **(c)**: Self-consistent potentials $\mathcal{V}(x)$ with a solid line in navy color, and electron confinement potential $\mathcal{V}_c(x)$ in black dashed line. Figure **(a)** corresponds to $n_d = 1.0{\times}10^{25}\,(1/\mathrm{m}^3)$ and figure **(c)** to $n_d = 4.5{\times}10^{25}\,(1/\mathrm{m}^3)$. For both figures the parameters $L = 10\,\mathrm{nm}$, $\xi = 0\,\mathrm{nm}$, and $\delta = 2\,\mathrm{nm}$ have been set. In both figures, the probability densities of some confined states have been included. The shaded region indicates the occupied states, and the maximum of said region corresponds to the energy Fermi level. Figure **(b)** represents the energy of the confined states as a function of n_d-parameter; the dashed line is the self-consistent Fermi level E_f.

significant increase in the Hartree potential due to the increase in the doped region going from $\delta = 1\,\text{nm}$ to $\delta = 5\,\text{nm}$ (black and red curves respectively); this modification explains the increase in the depth of the quantum well in Figure **3-2**(**c**) and the change in the shape of the barrier region because the potential takes values comparable to the barrier potential V_0 for points in the region $x < -5\,\text{nm}$ and $x > 5\,\text{nm}$ (see the red curve in Figure **3-5**(**b**)). The increase in the Hartree potential is due to the fact that the system increases the region of the doped layer δ, keeping the donor density n_d fixed in this region, this implies that there must be an increase in the number of charge carriers, this is evidenced by a much higher electron occupancy in excited states (as presented in Figure **3-2**(**c**)) thus increasing the charge density and therefore the electrostatic potential.

On the other hand, Figure **3-5**(**a**) shows an increase in the electrostatic potential caused by the increase in the well width, going from $L = 10\,\text{nm}$ to $L = 25\,\text{nm}$. Although there is no change in the donor density, the increase in the well width generates a decrease in the confinement and therefore, a decrease in the energy of each state, thus allowing a higher occupancy of states (see Figure **3-1**(**c**)), which implies a greater contribution to the charge density, which generates an effective increase in the electrostatic potential.

Finally, in Figure **3-5**(**c**) comparing the black curve that corresponds to $\xi = 0$ with the red curve that is for $\xi = 10\,\text{nm}$, the asymmetry originated in the potential of Hartree by the position of the delta layer that induces an asymmetry gives rise to a second potential well at the bottom of the conduction band as previously presented in Figure **3-3**(**c**) with asymmetric states. Note the increase in the intensity of the electrostatic potential with the change in the doped layer position, this is due to the fact that the system went from having a single well to having two wells and therefore a decrease in the confinement of the system was generated, and consequently, a decrease in the energy of each state. This implies a greater number of occupied states (see Figure **3-3**(**c**)) since the Fermi level remains fixed for the modification of ξ since the number of charge carriers per volume unit does not change. A consequence of the above is an increase in the charge density and therefore in the Hartree potential according to Poisson's equation.

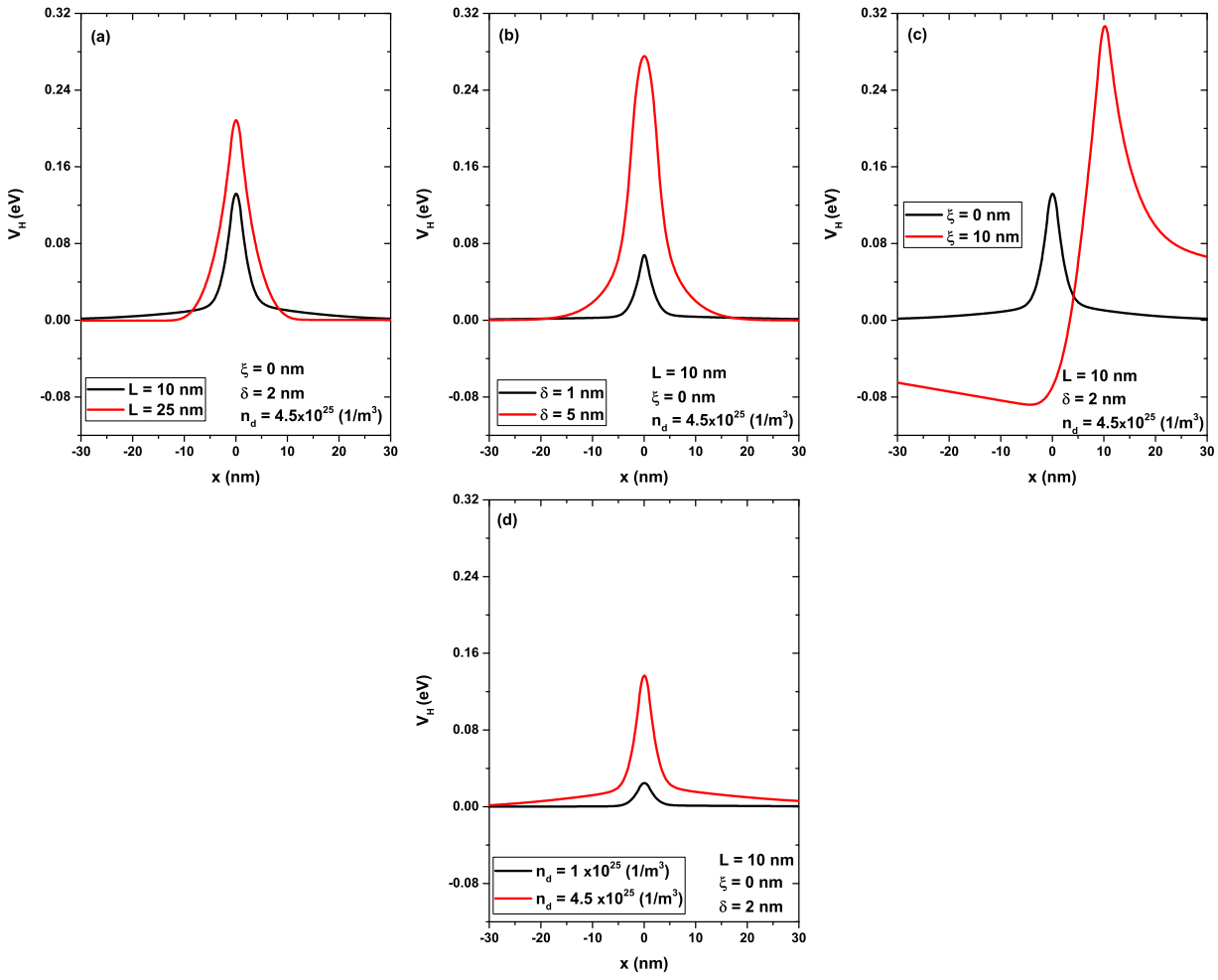

Figure 3-5.: Self-consistent Hartree potential as a function of x-position. In **(a)** varying the L, in **(b)** varying the δ, in **(c)** varying the ξ, and in **(d)** varying the n_d. In each case, when one parameter is changed, the others are set to $L = 10\,\mathrm{nm}$, $\xi = 0$, $\delta = 2\,\mathrm{nm}$, and $n_d = 4.5{\times}10^{25}\,(1/\mathrm{m}^3)$.

Figure **3-6** shows the electron density as a function of x-position. In **(a)** varying the L, in **(b)** varying the δ, in **(c)** varying the ξ, and in **(d)** varying the n_d. In each case, when one parameter is changed, the others are set to $L = 10\,\text{nm}$, $\xi = 0$, $\delta = 2\,\text{nm}$, and $n_d = 4.5{\times}10^{25}\,(1/\text{m}^3)$. Again all four figures have been put on the same scale to allow for better comparison. In Figure **3-6(a)**, the electron density is compared for two different widths of the quantum well. As the fact of increasing L does not generate changes in the donor density, therefore in magnitude, the density must remain fixed, only its distribution changes; that is, for $L = 10\,\text{nm}$, the electrons are more localized in the central region between -5 nm$< x <$5 nm. On the other hand, for $L = 25\,\text{nm}$, the electrons lose the location, now located in a much larger region between -12.5 nm$< x <$12.5 nm keeping the number of electrons per unit volume fixed. Additionally, as presented in Figure 3.1(c), the electron density for $L = 25\,\text{nm}$ must contain the contribution of two occupied excited states that have high probability density in regions close to each barrier, increasing the electronic density in these regions.

Figure **3-6(b)** compares the electron density for two widths of the doped layer $\delta = 1\,\text{nm}$ and $\delta = 5\,\text{nm}$. Since there is no change in the well width, the electrons are distributed mainly in the region between -5 nm$< x <$5 nm. The electron density magnitude is greater for $\delta = 5\,\text{nm}$ since the donor density in $n_d = 4.5{\times}10^{25}\,(1/\text{m}^3)$ and these are distributed in a greater volume, then the number of charge carriers must increase as clearly seen by comparing the red curve with the black one. Figure **3-6(c)** compares the electron density for two different positions of the same doped delta layer: $\xi = 0$ and $\xi = 10\,\text{nm}$, located 5 nm to the right of the edge of the well. In the case $\xi = 0$, again, the electrons are distributed inside the GaAs well, while in the case of $\xi = 10\,\text{nm}$, most of the electrons are already in the AlGaAs region located in the well generated by the doped delta layer. Although a part of electrons remains even inside the initial well, this distribution is because the well generated by the delta layer has a slightly greater width than the initial well that it is modified by the Hartree potential; this being sharper, and therefore the electrons tend to be in the region of least confinement (see Figure **3-3(c)**. Finally, Figure **3-6(d)** compares the electron density for two different donor densities in the delta layer $n_d = 1.0{\times}10^{25}\,(1/\text{m}^3)$ and $n_d = 4.5{\times}10^{25}\,(1/\text{m}^3)$ corresponding to the black and red curves respectively. In this case, the increase in n_d directly causes an

increase in the number of negative charge carriers that are concentrated inside the quantum well, which is only modified in its depth.

3.3. Linear optical absorption coefficient and EIT

The Figure **3-7** shows the absorption coefficient calculated according to the equation (2-55) between the states Ψ_0 and Ψ_1 (shaded curves. The absorption curves have been multiplied by 5) as a function of the incident photon energy. The unshaded curves correspond to the calculation of the EIT between the first three states of the system calculated via equation (2-139). In **(a)** varying the L, in **(b)** varying the δ, in **(c)** varying the ξ, and in **(d)** varying the n_d. In each case, when one parameter is changed, the others are set to $L = 10\,\text{nm}$, $\xi = 0$ $\delta = 2\,\text{nm}$, and $n_d = 4.5{\times}10^{25}\,(1/\text{m}^3)$. In Figure **3-7(a)** we see that the absorption coefficient corresponding to the system with $L = 10\,\text{nm}$ has a greater intensity than the one corresponding to $L = 25\,\text{nm}$; this is since the matrix element $|M_{01}|^2$ corresponding to the system with the smallest L is higher. On the other hand, the photon absorption occurs at a higher energy of 125.6 meV for $L = 10\,\text{nm}$ compared to the 97.3 meV of $L = 25\,\text{nm}$. This is to be expected since the states for a smaller L are further apart. As the L is increased, more states enter the system and confined states begin to come together, as can be seen in Figure **3-1**. In Figure **3-7(b)**, we see that the peak of the absorption coefficient for $\delta = 1\,\text{nm}$ occurs at 107.1 meV, while for $\delta = 5\,\text{nm}$ occurs at 143.2 meV; this is because increasing the width of the doped layer increases the Hartree potential and therefore the depth of the quantum well, causing the entry of new states and reduction of separation of already confined states, this behavior is evidenced in Figure **3-2**. In Figure **3-7(c)**, we see that the maximum peak of the absorption coefficient corresponds to the system with $\xi = 0$ for an energy of 125.5 meV, compared to the 42.7 meV of the delta layer located in the asymmetric system $\xi = 10\,\text{nm}$. The explanation for this behavior is evident from the analysis of Figure **3-3**, in which the states Ψ_0 and Ψ_1 are closer when the delta layer is in the center of the quantum well, whereas when the delta layer

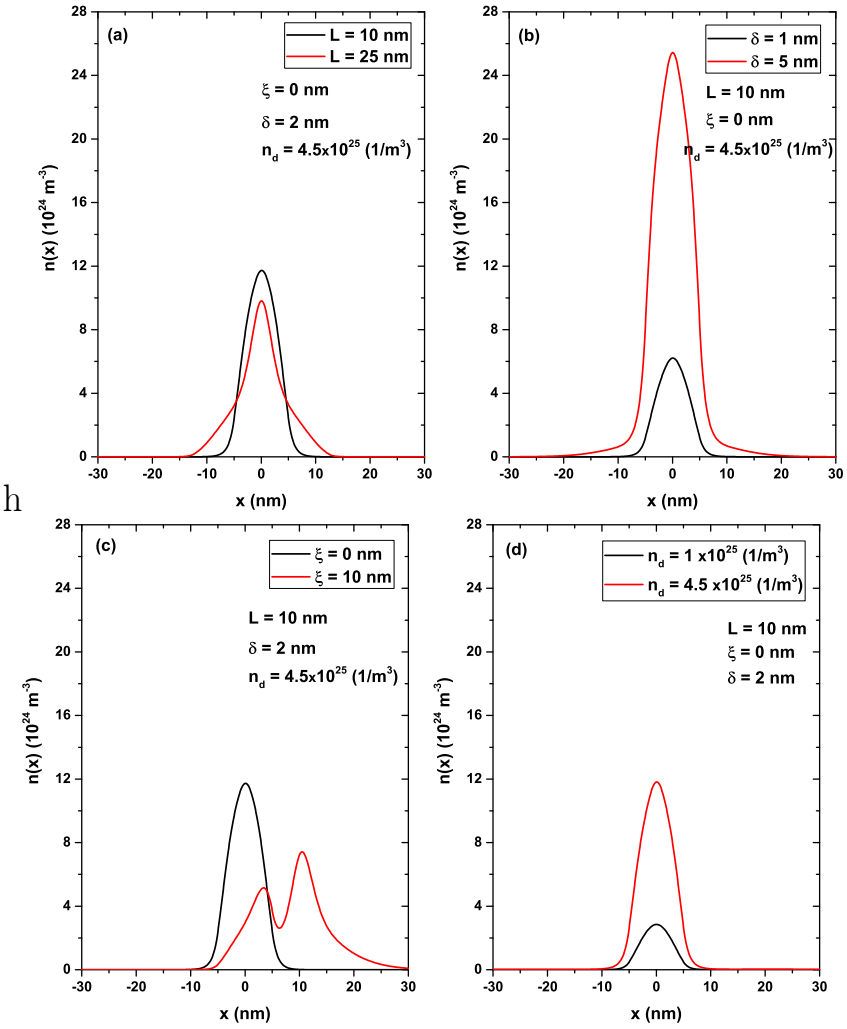

h

Figure 3-6.: Electron density as a function of x-position. In **(a)** varying the L, in **(b)** varying the δ, in **(c)** varying the ξ, and in **(d)** varying the n_d. In each case, when one parameter is changed, the others are set to $L = 10\,\mathrm{nm}$, $\xi = 0$, $\delta = 2\,\mathrm{nm}$, and $n_d = 4.5{\times}10^{25}\,(1/\mathrm{m}^3)$.

moves up to $\xi = 10\,\text{nm}$, a double quantum well system is generated, giving rise to the appearance of new confined states and a decrease in the transition energy between the ground state and the first excited state (see black and red curves of Figure **3-3(b)**). Note the significant difference in magnitude of the absorption peaks, the peak corresponding to $\xi = 0\,\text{nm}$ being much larger than that of $\xi = 10\,\text{nm}$, this is due to the fact that for $\xi = 0\,\text{nm}$, both the ground state and the first excited state are very localized inside the quantum well, however, when the system goes to $\xi = 10\,\text{nm}$, these states have a main location in different positions of x (see Figure **3-3(c)**), which decreases the matrix element $|M_{01}|^2$ and therefore the intensity of the linear optical absorption peak.

Finally, in Figure **3-7(d)**, the absorption peak is given at 95.6 meV for the system with $n_d = 1.0{\times}10^{25}\,(1/\text{m}^3)$ and of a significantly smaller magnitude than for $n_d = 4.5{\times}10^{25}\,(1/\text{m}^3)$ which takes a value of 125.7 meV. This behavior can be understood through Figure **3-5(c)**, which shows that the increase in the donor density causes an increase in the Hartree potential, and as a consequence of this, a deeper quantum well is generated (see Figure **3-4**), causing a separation of the confined states and particularly an increase in the transition energy corresponding to $\Psi_0 \rightarrow \Psi_1$. The increase in transition energy with increasing donor density for GaAs/AlGaAs QW was reported experimentally by Sasagawa *et al.* [8] in 1998.

The maximum absorption energy is presented for the set of parameters $L = 10\,\text{nm}$, $\xi = 0$, $\delta = 5\,\text{nm}$, and $n_d = 4.5{\times}10^{25}\,(1/\text{m}^3)$ with an energy of 143.2 meV represented by the shaded red curve of Figure **3-7(b)**.

According to the absorption coefficient, the EIT has been calculated, which, as stated in the theoretical framework, requires three confined states. In this calculation, the ground state and the first two excited states have been taken Ψ_0, Ψ_1, and Ψ_2 in a cascade configuration for each of the configurations presented in Figure **3-7**. The emergence of the EIT effect requires the coupling between the states $\Psi_0 - \Psi_1$ and $\Psi_1 - \Psi_2$, the Rabi frequency associated with the control field Ω_c, and the natural decay rates of the states γ_{01} and γ_{02} (see Table **3-1**). These decay rates are of great importance in this effect as they govern the magnitude of the resonant structures. Note that in each of Figure **3-7**(**a**-**d**), when the control field is turned on (through the frequency ω_p between

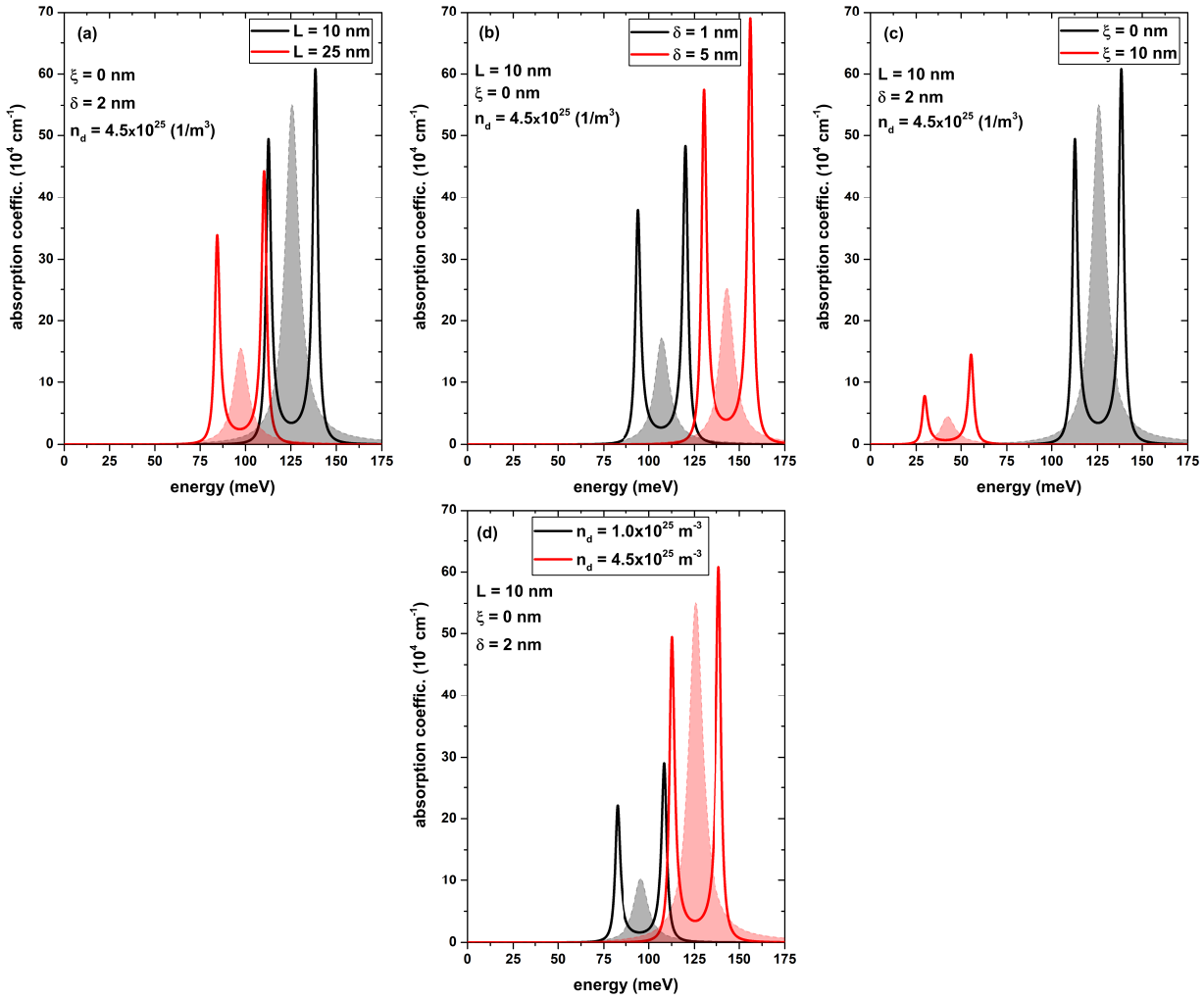

Figure 3-7.: In each figure, the shaded curves represent the absorption coefficient calculated according to the equation (2-55) between the states Ψ_0 and Ψ_1 (the absorption curves have been multiplied by 5), the unshaded curves correspond to the calculation of the EIT between the first three states of the system calculated using (2-139). In **(a)** varying the L, in **(b)** varying the δ, in **(c)** varying the ξ, and in **(d)** varying the n_d. In each case, when one parameter is changed, the others are set to $L = 10\,\text{nm}$, $\xi = 0\,\text{nm}$, $\delta = 2\,\text{nm}$, and $n_d = 4.5\times10^{25}\,(1/\text{m}^3)$.

states $\Psi_1 - \Psi_2$), the points of maximum absorption now change and they are points of minimum absorption (see red and black unshaded curves in Figures **3-7**(**a**-**d**)), that is, the system has become almost transparent for the frequency at which its absorption was maximum due to the coupling of a third state with an external control field. This is a quantum interference effect between three states with the application of two external electromagnetic fields as explained in Section 2.3. The behavior is complementary to that explained above for optical absorption, note that the EIT, like linear absorption, is proportional to the matrix element $|M_{01}|^2$, for this reason, the intensity of the EIT peaks change in magnitude proportionally to the absorption peaks.

In the calculation of the optical absorption, the system has been restricted to only two levels and interaction with a single mode of the electromagnetic field (semiclassical approximation). This consideration is valid whenever the two levels involved are in resonance or close to resonance with the external field and the remaining states are highly detuned with said field or are inaccessible states. It has been shown that, under some realistic approaches, by means of this scheme it is possible to extract essential physical characteristics of the systems under interaction with an external field [11, 12].
In the studied system, there is the advantage of having calculated the Fermi level for each layout, thus, the occupancy level of each of the electronic states of the system is clearly visualized. In this section, it is evident that the occupation for all the dispositions varies between 1 and 4 states, with the lowest energy, in addition, considering that the calculations have been carried out at room temperature, the upper states close to the Fermi level may correspond to semi-occupied states. This indicates that, regarding the calculation of optical properties such as linear absorption or EIT in this model, it does not make sense to calculate transitions between higher states (beyond the fourth excited state) since these correspond to unoccupied states.
For the case of an external electromagnetic field with an energy close to resonance between the ground state and the first excited state, in this system, the approximation at two levels for the absorption calculation or three levels for the EIT is not so bad as mentioned in the previous paragraph. The results show that the energy for the maximum absorption in general differs from the energy

difference between the excited states, allowing a reasonable approximation for such cases. On the other hand, the excited states that present energy differences close to the energy of the external field could present absorption and electronic transitions as long as the occupation of said states allows it. In the event of the latter, it would be expected to obtain an absorption peak in an energetic position very similar to the one calculated, but with a generally different intensity and amplitude, since the wave functions involved are modified and, therefore, the matrix elements will also change.

In the case of the 3-level model used, it is possible to demonstrate, in addition to the EIT, the generation of states that do not absorb or emit photons due to quantum interference as long as the system presents a superposition of two states initially, this type of state is known as dark states [11, 13]. An additional effect that could be evidenced is a lasing without inversion (LWI) effect, this can occur whenever the states are properly prepared [11, 14]. The additional effects mentioned can be carried out in the studied system based on the 3-level model used as future complementary works.

References

[1] Al, E. B.; Kasapoglu, E.; Sari, H.; Sökmen, I.; Duque, C. A.; Binding Energy and Absorption of Donor Impurity in Spherical GaAs/$Al_xGa_{1-x}As$ Quantum Dots With Konwent Potential, *Research square* **2021**.

[2] Bejan, D. Effects of electric field and structure on the electromagnetically induced transparency in double quantum dot, *Opt. Mater.* **2017**, *67*, 145-154.

[3] Al, E. B.; Kasapoglu, E.; Sari, H.; Sökmen, I. Optical properties of spherical quantum dot in the presence of donor impurity under the magnetic field, *Physica B* **2021**, *613*, 412874.

[4] Dakhlaoui, H.; Belhadj, W.; Durmuslar, A. S.; Ungan, F.; Abdelkader, A. Numerical study of optical absorption coefficients in Manning-like AlGaAs/GaAs double quantum wells: Effects of doped impurities, *Physica E Low Dimens. Syst. Nanostruct.* **2023**, *147*, 115623.

[5] Aleshchenko, Y. A.; Kazakov, I. P.; Kapaev, V. V.; Kopaev, Y. V.; Kornyakov, N. V.; Tyurin, A. E. Interference ionization of an impurity by an electric field in a system of quantum wells, *Jetp Letters* **1999**, *69*, 207–214.

[6] Dakhlaoui, H. , The effects of doping layer location on the electronic and optical properties of GaN step quantum well, *Superlattices Microstruct.* **2016**, *97*, 439-447.

[7] Dhafera, R. B.; Saidi, H.; Ridenea, S. Proposal of InP/AlInGaAs single delta quantum well for fiber-optic communications, *Optik* **2018**, *158*, 164-169.

[8] Sasagawa, R.; Sugawara, H.; Ohno, Y.; Nakajima, H.; Tsujino, S. Enhancement of intersubband transition energies in GaAs quantum wells by Si delta doping of high concentration, *Appl. Phys. Lett.* **1998**, *72*, 719-721.

[9] Haupt, R. Wendler, L.; Pechstedt, R. Depolarization shift in quasi-one-dimensional quantum-well wires, *Phys. Rev. B* **1991**, *44*, 13635-13640.

[10] Shtrichman, I.; Metzner, C.; Ehrenfreund, E.; Gershoni, D.; Maranowski, K. D.; Gossard, A. C. Depolarization shift of the intersubband resonance in a quantum well with an electron-hole plasma, *Phys. Rev. B* **2001**, *65*, 035310.

[11] Scully, M. O.; Zubairy, M. S. Quantum optics, *Cambridge University Press* **1997**, ISBN 9780511813993.

[12] Gerry, C.; Knight, P. Introductory Quantum optics, *Cambridge University Press* **2004**, ISBN 9780511791239.

[13] Lindberg, M.; Binder, R. Dark states in coherent semiconductor spectroscopy, *Phys. Rev. Lett.* **1995**, *75*, 1403-1406.

[14] Nikonov, D. E.; Imamoglu, A.; Scully, M. O. Fano interference of collective excitations in semiconductor quantum Wells and lasing without inversión, *Phys. Rev. B* **1999**, *59*, 12212-12215.

4. Conclusions

The effects of a doper layer on the optical absorption coefficient and the EIT in a GaAs/AlGaAs QW have been studied using a self-consistent coupling formalism between the Schrödinger, Poisson, and charge neutrality equations. The induced modification to the conduction band due to the electrostatic potential originated by the charge carriers has been considered. Modifications in the well width increase the number of confined electron states, which generates modifications in the electronic density and, therefore, in the linear absorption coefficient. Consequently, an appreciable decrease in the intensity of the absorption peak and a redshift in the resonance energy have been observed; a similar behavior is evident in the EIT. It has been found that, by increasing the doped layer width, a deeper QW is generated, and, as a consequence of this, the confined state's occupation is significantly increased; a similar effect is observed on the transition energy between them. An immediate consequence of the above is an increase in the electron density, the electrostatic potential, and a blue shift with higher intensity absorption peaks. On the other hand, when the position of the doped delta layer is modified, keeping its width fixed at 2 nm, and the three-dimensional doping density at $n_d = 4.5\times10^{25}\,(1/\mathrm{m}^3)$, the self-consistent potential profile becomes completely asymmetric and gives rise to a double-well system. These modifications increase the number of confined states simultaneously with a decrease in transition energies. Direct consequences on the optical properties of the system are observed: redshift of the peak position and a significant decrease in the intensity of both the linear absorption coefficient and the EIT. To finalize the system characterization, modifications were made in the donor density, causing an increase in the electrostatic potential, electronic density, and the number of occupied states. In this case, the transition energy between states is higher, and therefore, there is a blueshift of the resonance peak in linear absorption and a clear increase in its intensity. In this work,

the possibility of tuning the optical properties, such as the linear absorption coefficient and the EIT has been demonstrated using modifications in various geometric and non-geometric system parameters, including the donor density.

The possibility of tuning the system through the EIT has allowed potential applications as mentioned at the end of section 2.3, in the field of quantum information technology the EIT has been identified as a possibility that facilitates the processing of quantum information of some qubits, in the same way, the possibility of controlling the speed of light in optomechanical crystals of the order of nanometers has been demonstrated. In the field of medicine, EIT has recently been used as a type of biosensor, with good efficiency for the detection of some cancer cells. In the field of optoelectronics, the possibility of tuning the optical absorption coefficient by means of structural parameters and external fields in QWs has been demonstrated, allowing even applications in the terahertz range. These are some of the potential applications that the type of heterostructures characterized in this work could have, since they present the possibility of modulating the characteristics of optical absorption and EIT.

Perspectives

As perspectives for the future, it is intended to apply the method to a system with three-dimensional confinement (such as a quantum dot for example) and to study the optical response considering excitonic properties (which implies resolving not only the electron but also the hole and its interaction), initially work on a system with multilayer spherical symmetry and extend the calculations for a system with other types of symmetry (ellipsoid for example).

A. Python Self-Consistent Code

This section includes the self-consistent code used for the work calculations.

```
import numpy as np
import matplotlib.pyplot as plt
from scipy.sparse import diags
from scipy.sparse.linalg import eigs
from scipy.integrate import solve_bvp
from scipy import optimize
from findiff import FinDiff

####### Parameters #########
L = 10       # well length in nm
Ldelta = 2*10**(-9)      # delta layer length in m
Ld = 2           # delta layer length in nm
hbar = 1.054*10**(-34)      # reduced Plank constant en J*s
m0 = 9.1093837015*10**(-31) # free electron mass in kg
qe = 1.602*10**(-19)      # electron charge in C
kb = 1.380649*10**(-23)     # Boltzman constant in J/K
Vba = 0.228     # potential height in eV
meff = 0.067*m0  # electron effective mass GaAs
eps0 = 8.8542*10**(-12)     # vacuum permittivity in F/m
epsr = 12.35  # relative permittivity GaAs
T = 300  # temperature in K
nd3D = 4.5*10**(25)         # electron density in 1/m^3
```

```
nd2D = nd3D*Ldelta          # electron density in 1/m^2
Cte1 = hbar**2/(2*meff)/10**(-18)/qe  # in eV*nm^2
Cte2 = (meff*kb*T)/(np.pi*hbar**2)   # in 1/m^2
infy = 100                           # system infinite
zi = 0                          # delta layer position zi (nm)

################################################
N = 2001 # number of points to calculate
x = np.linspace(-infy, infy, N) # define our grid
dx = (2*infy)/(N-1)
################################################
# initial potential
def V1(z,L):
if -L/2<=z<=L/2:
return 0.0
else:
return Vba
def V2(z,L):
if -L/2-0.8*infy <=z<= L/2+0.8*infy:
return 0.0
else:
return 10
def V(z,L):
return V1(z,L)+V2(z,L)
##############################################################
##############################################################
# delta layer difining
def g1(z):
return np.piecewise(z, [z<=-Ld/2+zi, z>-Ld/2+zi], [nd3D, 0])
def g2(z):
return np.piecewise(z, [z<=Ld/2+zi, z>Ld/2+zi], [nd3D, 0])
def Nd(z):
return g2(z)-g1(z)
##############################################################
```

```
Naut = 100 # maximum number of iterations
tol = 0.1 # tolerance for the Fermi level in meV
LL = 10 # initial width of the Well
longWell = []
autovalores = []
Efj = []
while LL < 25.5: # maximum width of the well in nm
# Writing the potential as an array
V00 = [V(i,LL) for i in x]
V0 = np.array(V00)
#****************************************
jj = []
error = []
Ef_int = []
Vn = np.zeros(V0.size)
for j in range(0,Naut+1):
if j == 0:
Vn = V0
else:
Vn = 0.95*Vn + 0.05*(V0 - y/qe) # new potential in eV

H = -Cte1*FinDiff(0, x[1]-x[0], 2).matrix(x.shape) + diags(Vn)
energies, states = eigs(H, which='SM', k=10)
def Psi(jj,z):
I2 = []
for i1 in range(0,N):
xp = -infy + i1*dx
fun = abs(float(states[:, jj].real[round(float(xp + infy)/dx)]))**2
I2.append(fun)
Norm = sum(I2)*dx*10**(-9)
return float(states[:, jj].real[round(float(z + infy)/dx)])/np.sqrt(abs(
def Ndd(Ef,nn):
I=[]
for i2 in range(0,nn+1):
```

```
valor = Cte2*np.log(1 + np.exp(qe*(Ef-energies[i2])/(kb*T)))
I.append(valor)
total = sum(I)
return total
def f(Ef):
return nd2D - Ndd(Ef,3)
Eff = np.real(optimize.newton(f, 0.1))
def n(z1,nn):  # electron density in 1/m^3
II=[]
for i3 in range(0,nn+1):
valor = np.real(Cte2*np.log(1 + np.exp(qe*(Eff-energies[i3])/(kb*T)))*abs(Ps
II.append(valor)
total = sum(II)
return total
A = np.zeros((N, N))
A[0, 0] = 1
A[N-1, N-1] = 1
for i4 in range(1, N-1):
A[i4, i4-1] = 1
A[i4, i4] = -2
A[i4, i4+1] = 1
b = np.zeros(x.size)
for i5 in range(1, N):
b[i5] = dx**2*float(qe**2*(n(x[i5],3) - Nd(x[i5]))/(eps0*epsr))*10**(-18)
y = np.linalg.solve(A, b)  # Hartree potential in J
print('L_well=',LL, 'iter=', j, '  Ef = ', Eff)
Ef_int.append(Eff)
if j>0 and np.abs(Ef_int[j]-Ef_int[j-1])*1000 < tol:
break
print('*****************************************')
Efj.append(Eff)
autovalores.append(energies)
longWell.append(LL)
LL = LL + 1.0
```